High Frequency Analysis of Microwave components for High Power RF Sources using Finite element analysis software

A Major Project Report

Submitted in Partial Fulfillment of the Requirements for the degree of

MASTER OF TECHNOLOGY

IN

ELECTRICAL ENGINEERING

(POWER APPARATUS & SYSTEMS)

By

Thalla Suryadhar Reddy

(04MEE019)

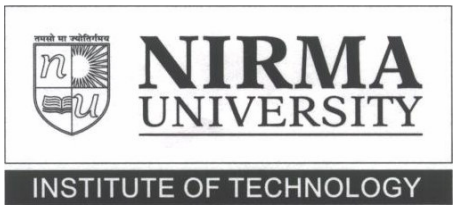

Department of Electrical Engineering
INSTITUTE OF TECHNOLOGY
NIRMA UNIVERSITY OF SCIENCE & TECHNOLOGY,
AHMEDABAD 382 481

MAY 2006

Certificate

This is to certify that the Major Project Report entitled "**High Frequency analysis of Microwave components for High Power RF sources using Finite Element analysis software**" submitted by **Mr. T. Suryadhar Reddy** (**04MEE019**), towards the partial fulfillment of the requirements for the award of degree in Master of Technology (Electrical Engineering) in the field of Power Apparatus & Systems of Nirma University of Science and Technology is the record of work carried out by him under our supervision and guidance. The work submitted has in our opinion reached a level required for being accepted for examination. The results embodied in this major project work to the best of our knowledge have not been submitted to any other University or Institution for award of any degree or diploma.

Date:

Project Guides:

Industry Guide:

Mr. N Ravi Prakash
Scientist - SD
Institute for Plasma Research
Gandhinagar

Institute Guide:

Mrs. Rajal H Patel
Assistant Professor
Department of Electrical Engineering
Institute of Technology
Nirma University
Ahmedabad

HOD
Department of Electrical Engineering
Institute of Technology
Nirma University
Ahmedabad

Director
Institute of Technology
Nirma University
Ahmedabad

ACKNOWLEDGEMENT

I would like to thank the Institute for Plasma Research for granting my dissertation work. I would give my sincere thank to Mr. N Ravi Prakash, CAE-coordinator at Institute for Plasma Research to consider me in project.

This thesis owes its completion to the encouragement and contributions by a number of people, which include scientists and professors. I thank all of them collectively here.

Next, I would like to express my sincere gratitude to some specific persons from whom I learnt many things in high frequency, which help me to complete my dissertation. The foremost amongst them are Mr. N Ravi Prakash (Scientist-'SD', IPR), Ms. Ranjana Gangradey (Scientist-'SD', IPR) and Mrs. Rajal H Patel (Assistant Prof., Nirma University). I thank them for introducing me to this novel high frequency analysis.

I would like to thank to Dr. D Bora (Professor, IPR) and Dr. S K Pathak (Scientist-'SE', IPR) for encouraging me towards the new problems and its application during the dissertation. I also like to thank Mr. K Sathyanarayana (Scientist-'SD', IPR), Mr. B K Shukla (Scientist-'SD', IPR) at IPR for their support during the dissertation.

I would like to express my sincere gratitude to Prof. U A Patel, Prof. B B Kadam, Mr. J G Jamnani, Mr. S C Vora, Mr. C R Patel and other staff members of Electrical Engineering Department of Nirma University of Science and Technology.

I sincerely thank Prof. Dr. M V Kartikeyan of Indian Institute of Technology, Roorkee for stimulating discussions and useful suggestions.

I sincerely thank my parents for taking care of each and every fact with personal attention, which helped in successful completion of the dissertation work.

Suryadhar Reddy T

ABSTRACT

Tokomaks are the fusion devices where plasma is produced and confined under magnetic confinement methods. A promising method of heating the plasma is carried out by the launching of high frequency microwaves. The RF power sources can be klystrons, gyrotrons and gyroklystron which include the leading edge technologies with an advanced engineering design. The simulation and analysis of various subsystems of gyrotron like cavity, super conducting coil, RF window, and so on are required for developing an efficient RF source. The project work includes the modeling and analysis of the subsystems using finite element methods with high frequency module of ANSYS software. The work includes a set of benchmarks problems for existing RF components and the latest RF sources that is developed in the country.

ANSYS is the software that has been keenly programmed with many sorts of problem in electromagnetic. ANSYS gives more accurate and better solution for the actual geometry in existence.

CONTENTS

LIST OF FIGURES

Chapter 7

Chapter 8

NOMENCLATURE

AC	Alternating Current
AD	Computer-aided design
AE	Computer-aided engineering
ECRH	Electron cyclotron resonance heating
EA	Finite element analysis
EM	Finite element method
UI	Graphical user interface
IEEE	Institute of electrical and electronics engineers
IPR	Institute for plasma research
RF	Radio frequency
TE	Transverse electric
TM	Transverse magnetic
2D	Two dimensional
3D	Three dimensional
B	Magnetic flux density
$\mathbf{B_{sum}}$	Resultant magnetic flux density
c	Free space velocity of light
e	Electron charge
E	Electric field intensity
f	frequency
$\mathbf{f_c}$	Cut-off frequency(of a wave guide)
H	Magnetic field intensity
$\mathbf{H_{sum}}$	Resultant magnetic field intensity
I	Current
J	Current density
m	Electron mass
Q	Quality factor
r	Radius
R	Resistance
$\mathbf{V_{II}}$	Axial beam velocity

α	Attenuation constant
β	Phase constant
γ	Wave guide propagation constant
ε_o	Dielectric constant for free space
ε_r	Relative dielectric constant
δ	Skin depth
λ	Wave length
λ_c	Cut-off wave length
μ	Permeability
μ_r	Relative permeability
ρ	Resistivity
σ	Conductivity
ω	Resonance frequency

CHAPTER 1 INTRODUCTION

Millimeter waves (ν = 30 - 300 GHz) occupy a somewhat unique position in the electromagnetic spectrum in that there are very few types of sources in this frequency regime, which are capable of high-power operation. Lasers are generally not capable of efficient operation beyond mid-infrared wavelengths, and conventional RF sources also face serious handicaps due to the inverse frequency scaling of their components. Klystrons, TWTs, BWOs, and other slow-wave devices all have interaction structures (resonant cavities or helixes, for example) whose sizes are on the order of a wavelength. As the operating wavelength decreases, it becomes more and more difficult to manufacture and align the fragile components; more importantly, their small size results in the inability to handle high power levels or current densities before ohmic heating and/or arcing result in failure of the device. As a result, such slow-wave sources are limited to frequencies of less than 100 GHz.

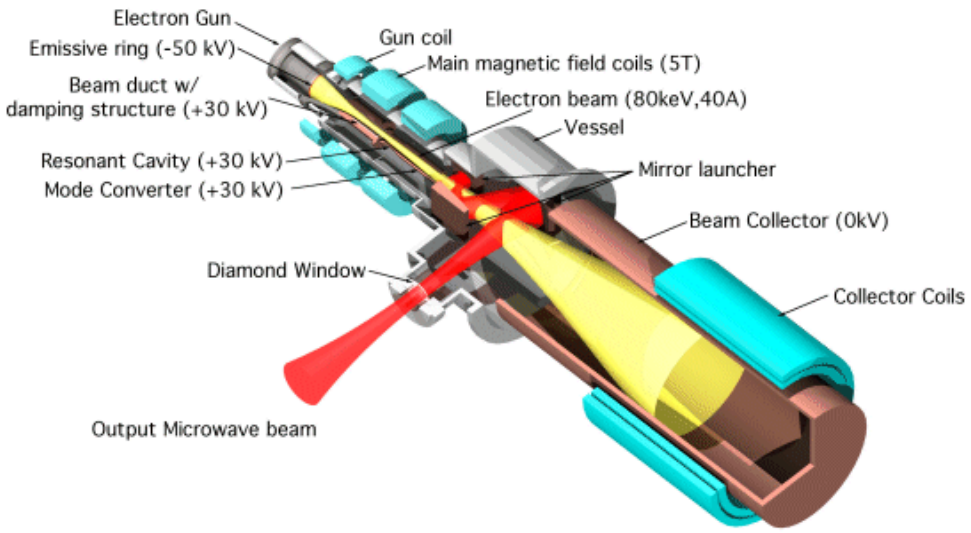

Figure 1-1: Gyrotron with radial output

Gyrotrons, or electron cyclotron masers, bridge this gap between slow-wave devices and lasers, and are capable of producing very high output power with theoretical efficiencies of forty percent, thus making them an important source within the millimeter wave regime. The principles, which allow this remarkable performance, are reasonably simple. An energetic annular electron beam is produced and passes toward a resonant cavity, which is located in a region of intense magnetic

field oriented along the beam axis. A schematic of a gyrotron is shown in Figure 1-1 and Figure 1-2. The magnetic field causes the electrons to gyrate in small orbits about their original path, producing a net helical trajectory. As a result of this helical motion, the electrons emit radiation; if the magnetic field and cavity are properly matched to the beam parameters, this radiation will couple into a resonant cavity TE mode and amplify it. With sufficiently good coupling and proper design, large amounts of monochromatic radiation can then be extracted. Since there is no requirement to couple into the fundamental waveguide mode, the interaction cavity can be significantly larger than the wavelength of the output radiation, thus avoiding the frequency-scaling problem associated with slow-wave devices.

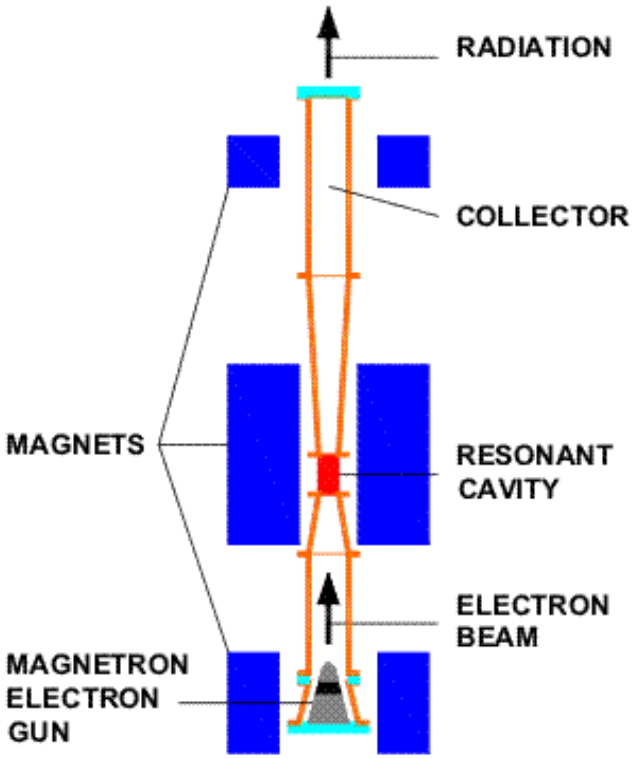

Figure 1-2: Gyrotron with axial output

Historically, gyrotron research has been driven by a need for ECRH of fusion plasmas. Towards this end, very high power devices have been developed at frequencies ranging from 90 to 170 GHz. In recent years, the technology has matured to the point where other applications such as material processing, millimeter-wave radar systems. This thesis focuses on analysis of the sub-systems of the gyrotron, which is used for ECR heating of fusion plasma.

Literature review is presented in the chapter two. An introduction to the theory of gyrotron is presented in chapter three. It also describes the project work. Chapter four describes the performance goals and design parameters of the CW 200KW 42GHz gyrotron, CW 1MW 110GHz gyrotron. Chapter five describes the static electromagnetic analysis of super conducting coils. Chapter six describes the high frequency modal analysis of the cavity. Chapter seven describes the coupled field analysis of the pillbox cavity. Chapter eight includes the discussion and conclusion. Chapter nine presents the future scope.

CHAPTER 2 LITERATURE REVIEW

The dissertation work is focused on doing the high frequency analysis of microwave components for high power RF sources using finite element analysis software. The finite element analysis software which is used in the dissertation work is ANSYS software. The high power RF sources which are considered for the analysis are CW 200 KW 42 GHz and CW 1 MW 110 GHz gyrotrons.

- Gyrotron oscillators—Their principles and practice [*1*]

  This textbook explains about the gyrotron oscillators with the help of both theory and experimental results. It explains about the subsystems of the gyrotron and factors affecting them. The gyrotrons with different frequencies and power levels are explained with its design. The frequency tunable gyrotrons are also described.

- Microwave engineering-Passive circuits [*10*]

  Cavity is one of the important subsystems of the gyrotron. Chapter-9 of this book explains the basic fundamentals and different types of the cavities. The effect of the dimensions and mode on the quality factor and resonant frequency for the standard cavity models are described.

- Design of a 42 GHz 200 kW gyrotron operating at second harmonic [*7*]

  This IEEE papers consists of the simulation results of the 42 GHz, 200 KW CW gyrotron. The different dimensions of the various subsystems are given. The results from this paper are taken as benchmark results for thesis analysis. The results are verified using ANSYS software.

- Use of ANSYS for electromagnetic analysis of RF cavities [*4*]

  This paper explains in detail how to perform the electromagnetic analysis of RF cavities in ANSYS software. It also explains where to apply the boundary conditions, how to do meshing for accurate results.

- A coupled-field analysis on RF cavity [*3*]

  This paper consists of analysis methodology to perform the coupled-field analysis. It explains the procedure with the help of a pillbox cavity. These results are taken as benchmark for the macro.

- Plot of modal field distribution in rectangular and circular wave guides [*2*]

  This IEEE paper gives the basics of patterns of various modes in rectangular and circular waveguides.

- www.ansys.com [*11*]

  ANSYS is the software that has been keenly programmed with many sorts of problem in electromagnetic and high frequency. ANSYS gives more accurate and better solution for the actual geometry in existence. From the help manual of ANSYS the steps for solving the high frequency analysis is understand.

The various books presented above are available at library of IPR [*Institute for Plasma Research*] and Nirma University.

CHAPTER 3 THE PROJECT WORK

3.1 Significance of the project

Dissertation title

High frequency analysis of microwave components for high power RF sources using finite element analysis software.

Significance

The gyrotron or electron cyclotron resonance maser is a novel and important microwave and millimeter wave generation device. Gyrotrons are currently being used for electron cyclotron resonance heating (ECRH) of plasmas in plasma fusion experiments. The simulation and analysis of various subsystems of gyrotron like cavity, super conducting coil, RF window, and so on are required for developing an efficient RF source. The project work includes the modeling of the subsystems (cavity & super conducting coil) using finite element methods with high frequency module of ANSYS software.

3.2 Gyrotron theory

The theory of electron cyclotron resonance devices can be quite complex, as it involves not only the problem of electromagnetic fields inside a cavity but also the interaction of those fields with a beam of weakly relativistic electrons which in turn interact with one another and produce their own fields. In fact, it is necessary to make a number of approximations before any sort of tangible, analytic physical result can be obtained. This chapter presents an introduction to gyrotron theory along those lines, including a discussion of the mechanisms by which an annular electron beam can form bunches and amplify an appropriate resonant cavity mode.

3.2.1 Electron beams

A schematic drawing of a typical gyrotron is shown in Figure 3-1. The energy source for these devices is an electron beam, which propagates through the interaction cavity as shown in the figure. For this reason, the theoretical discussion will begin by considering the production and propagation of electron beams through a typical gyrotron.

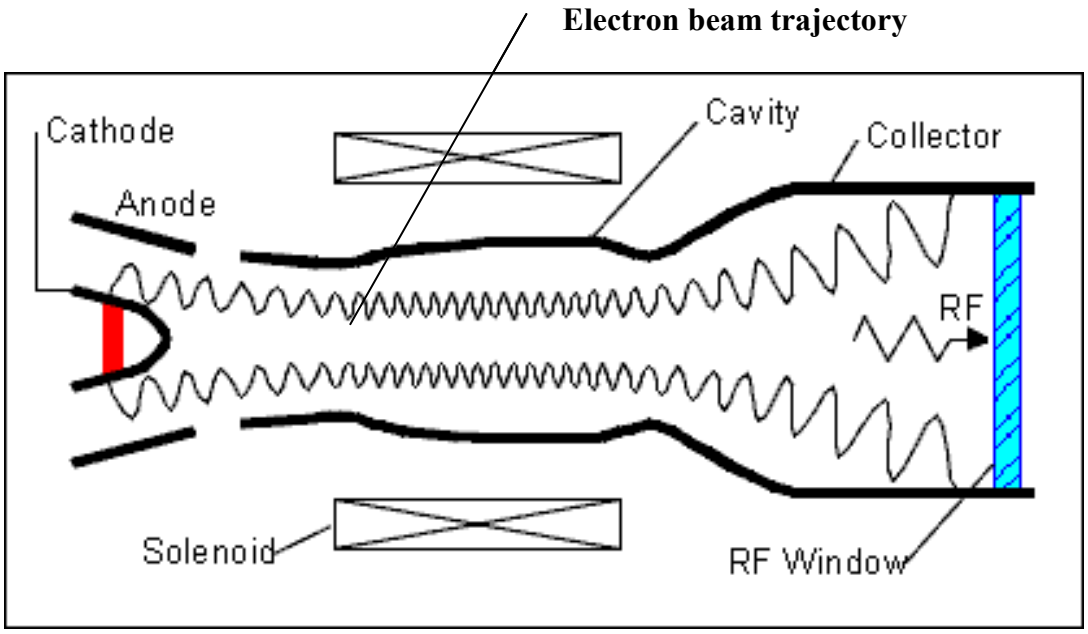

Figure 3-1: Schematic drawing of a gyrotron

3.2.2 Magnetron injection guns

Most gyrotrons make use of a thermionic electron gun to provide high-current annular electron beams. The electron-emitting cathode for such a gun typically consists of a matrix material (tungsten, for example), which is impregnated with rare-earth metals, and other materials in order to reduce the effective work function. When an AC current heats the emitter, usually, some electrons gain sufficient thermal energy to overcome the work function barrier and are ejected into free space. The emitting cathode is biased to a large negative voltage (10-100 kV) relative to the hollow anode, so the ejected electrons are immediately accelerated toward the anode. Emitters for Gyrotron guns are typically ring or bell-shaped, which results in the formation of a hollow or annular electron beam. This shape is superficially similar to the interaction region of a magnetron, which is responsible for the term often used to refer to these devices: magnetron injection gun.

3.2.3 Beam transport and gyration

The gyrotron interaction draws energy only from the transverse (rotational) velocity of the beam, which is quite small in the gun region. As a result, the large axial beam velocity (v_{II}) acquired from the accelerating potential must be partially

converted into transverse motion before energy extraction can occur. This is done by means of a strong solenoid magnetic field. As the electron beam leaves the cathode, it enters a region of rapidly increasing magnetic field, and is compressed. In addition to being compressed, the field gradient near the gun also causes the beam to begin to rotate, as the Lorentz magnetic force contains the cross product of the electric and magnetic fields.

As soon as the electrons acquire a velocity perpendicular to the axial magnetic field, they begin to feel a magnetic force in accordance with the Lorentz law. This results in the establishment of a circular orbit with angular frequency. The result of the superposition of this circular gyration upon the axial motion due to the anode is a helical path about a fixed guiding center. This is shown in figure 3-2. The radius of this path is small compared to the beam thickness, however, so the overall form of the electron beam remains annular as it propagates down the tube.

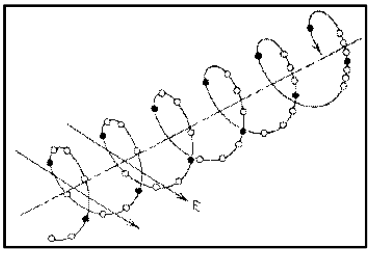

Figure 3-2 Gyration of electrons

Once the spent beam leaves the interaction cavity, it spreads out due to the decreasing axial magnetic field. After some distance, it is collected by a fixture near the end of the vacuum tube and returned to the power supply in order to complete the circuit. In the simplest design, the collector is grounded, but higher efficiency can be achieved by maintaining the potential at a negative value, thus decreasing the energy, which much is imparted to the electrons by the beam power supply. This setup, known as a depressed collector, can increase the overall efficiency of the tube by a significant amount and also results in a smaller (and therefore cheaper) beam power supply. However, it also complicates the arrangements for microwave transmission and coolant supply due to the potential difference between the collector and ground. As a result, this approach is used only on high-power tubes where efficiency is of critical concern.

3.2.4 Cyclotron resonance and power generation

3.2.4.1 Cavity fields

Gyrotron interaction cavities are typically cylindrical, with tapers of various sizes and lengths on either end to aid in mode selection. Such a cavity is capable of supporting a large number of resonant electromagnetic modes, but gyrotrons are typically operated near cutoff, so TM modes are generally suppressed in favor of TE modes. Experience has shown that semi-tapered gyrotron cavities are best modeled by a field profile.

3.2.4.2 CRM Electron bunching

In order to understand the methods by which an annular electron beam of the type described in section 3.1 can amplify a TE cavity mode, it is convenient to consider a small ensemble of electrons orbiting about the same guiding center. In the absence of any electric fields, the electrons in this beamlet will orbit the guiding center with an angular frequency. If a transverse electric field is present, the electrons feel an additional force qE, which will cause some electrons to accelerate, and others to decelerate depending on the relative phase of the electric field. Since the cyclotron frequency is inversely proportional to γ, the frequency will decrease for accelerated electrons and increase for decelerated electrons, resulting in phase bunching. If the electric field frequency is exactly equal to the electron cyclotron frequency, this bunching process will continue until the entire beamlet is bunched at a zero-field phase point. In order to extract power, the bunch must be formed at a field maximum; this is accomplished by a slight tuning of the axial magnetic field so that the cyclotron frequency is slightly lower than the RF frequency. When this condition is met, the

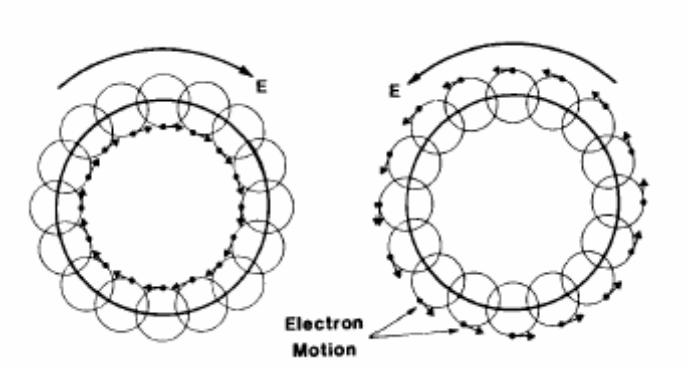

Figure 3-3: Field/Electron Bunch Interactions

bunches orbit in phase with the electric field and give up rotational energy to the field. A diagram of this condition is shown in Figure 3-3; the entire electron beam is shown, with the smaller circles representing the Larmor radii of each beamlet. Once a beamlet has become bunched in phase with a cavity mode, it gives up its rotational kinetic energy to the mode, thus increasing the field strength and promoting more bunching. This nonlinear feedback process results in a rapid amplification of the dominant mode.

3.2.5 Gyrotron operating conditions

Based on these arguments, as well as extensive linear and nonlinear calculation, several criteria can be set forth as required for efficient gyrotron operation.

Frequency matching: The frequency condition for amplification of the TE_{mp} mode in a non-harmonic gyrotron is given by the following expression, where ω is the cavity resonant frequency

$$\omega - k_{ll} v_{ll} = \omega_c = \frac{eB_{cavity}}{m\gamma}$$

Beam radius: The radius of the annular electron beam should correspond to a maximum of the transverse electric field for rapid bunching to occur:

$$r_{beam} = \frac{v_{m\pm1,s}}{v_{mp}} r_{cavity},$$

Where, ‘s’ is a small positive integer.

Beam quality: Efficient bunching and power extraction requires a high-quality electron beam; the velocity spread must be small in both the axial and transverse directions. If this is not the case, then the electrons will be unable to form bunches due to their differing velocities. Finally, the electron beam current density should be roughly constant around the annulus. If these three conditions are met, theory predicts that a gyrotron oscillator should be able to produce copious amounts of microwave power with efficiencies up to 40 percent. Furthermore, these efficiencies are achievable for high-order modes as there is no requirement to couple into the

fundamental resonance of the interaction cavity. This is what gives gyrotrons such an advantage over slow-wave devices in the millimeter and sub-millimeter wavelengths.

3.3 Basic concepts of the finite element method

There are several engineering problems for which we are not able to find exact solutions. This incapacity may derive either from the complex form of the differential equations that represent the problem that is being studied, or from the difficulty of imposing particular boundary and initial conditions that need to be respected.

To solve these problems, a solution might be the use of numerical approximations. Unlike analytical solutions, that represent the exact behavior of the system in any point within the system itself, numerical solutions approximate the behavior by considering a finite number of variables that correspond to the value of the function we are looking for in a discrete number of points, called nodes.

The first step in a numerical procedure, once the problem has been defined, is the discretization. This operation consists in dividing the medium, or structure, in a finite number of nodes and small sub-regions, that take the name of elements.

There are two main categories of numerical methods:

1) Finite difference method;

2) Finite element method;

With the finite difference method the differential equation is written for each node, and the derivatives are substituted by finite differences. This kind of approach gives us result as a set of simultaneous linear equations. Although this method is quite simple to understand and to use for solving not too complex problems, its application becomes rather complicated for the solution of problems with more complex geometries and boundary conditions, as well as with problems in which the materials do not have isotropic properties.

The finite element method uses integral formulations, instead of finite differences, to create a system of algebraic equations. More specifically this method assumes a continuous function to represent the solution for each element. The complete solution is then generated by correcting or assembling the individual solutions, allowing for continuity at the inter elemental boundaries. The finite element method is a numerical procedure that may be used to solve a great variety of

engineering problems: static, dynamic, linear or non-linear problems of structural, thermal, fluid dynamics and electromagnetic analyses.

3.4 ANSYS

ANSYS is a finite element numerical code with a great number of options, with which it is possible to perform structural, thermal, fluid dynamics and electromagnetic analyses. The recent versions of this software have many windows, among which a graphical user interface (GUI), dialogue boxes and tool bars. The commands may be given either with the GUI or by writing directly the command in the command line. The use of the graphical interface is easier to learn, more intuitive, and in some cases quicker. Anyway it is often preferable to use the command line for several reasons. First of all it gives the possibility to implement packets of functions to be executed in an iterative or sequential way, secondly it gives the possibility to create macros able to execute particular functions for which direct commands do not exist, and finally it gives the possibility to store and to transfer a project or an analysis in the form of a simple text file.

The ANSYS simulator can also perform coupled-field analyses involving two or more different disciplines, i.e. it is able to perform a complete analysis of a structure studying different physical variables and eliminating the problem of transferring data from an analysis to the next.

Even though this direct analysis is very useful, easy to use and fast, it does not give the possibility to check the results of the simulation, and it might therefore lead to some perplexity on its reliability. For this reason it is preferable, whenever possible, to perform separately each single analysis referring to different fields of physics, because a procedure of this sort is definitely easier to keep under control.

CHAPTER 4 DESIGN SUMMARY

Although this thesis project was begun after the design of the CW 42 GHz 200KW, CW 110GHz 1MW gyrotron had been completed, it is still worthwhile to describe the design parameters of the tube, both as an example of the theoretical presentations presented in Chapter 3 and to provide a framework by which the experimental results presented in the next Chapters may be interpreted. The technical specifications of the gyrotrons used for analysis are shown in Table 4.1.

Table 4.1

Technical Specification of the CW gyrotrons

Particular	**Specification for 42GHz**	**Specification for 110GHz**
Frequency	42 ± 0.05 GHz	110 ± 0.05 GHz
Output power	200 KW	1 MW
Pulse duration	CW	CW
Efficiency	35 %	-----
Wall loading	< 0.6 KW/Cm2	< 2 KW/Cm2
Beam voltage	65 KV	74.5 KV
Beam current	10 Amps	42 Amps
Gun type	MIG (Magnetron injection gun)	MIG
Interaction circuit	Weakly tapered cavity	Weakly tapered cavity
RF Output	Axial window collection	Axial window collection
Output mode	$TE_{4\,2}$	$TE_{28\ 8}$
Guiding system	Super conducting magnet	Super conducting magnet
Cooling	Liquid (Deionized water)	----

4.1 Cavity design parameters

A magnetic field of approximately 0.814T, 4.30T was selected for the 42 GHz, 110 GHz gyrotrons respectively. This magnetic field corresponds to an electron larmor frequency of approximately 42 GHz & 110 GHz. Design studies for 42 GHz gyrotron were carried out in early 2004. A preliminary design has been carried out on the 110 GHz gyrotron. A chief concern in selecting an appropriate cavity mode and Q was to avoid excessive ohmic heating of the interaction cavity due to large cavity fields while maintaining good coupling efficiency in order to minimize thermal loads on the collector from high beam current. Based on these considerations, the $TE_{4\,2}$ & $TE_{28\,8}$ modes were selected as the operating mode of choice respectively. As linear studies showed that these modes results in optimum coupling between the electron beam and cavity RF field. Cavity design parameters are shown in Table 4.2.

Table 4.2

Gyrotron cavity design parameters

Specification	**For 42 GHz**	**For 110 GHz**
Mode	TE_{42}	$TE_{28\,8}$
Frequency (GHz)	42	110
Magnetic field (T)	0.814 T	4.3 T
Diffractive Q	1131	992
Cavity radius (mm)	10.55	26.09
Input taper L_1 (mm),θ_1(°)	45, 2.5°	24, 2.5°
Uniform midsection L_2 (mm),θ_2(°)	50, 0°	19, 0°
Output taper L_3 (mm),θ_3(°)	45,3.5°	24, 3.5°

4.2 Magnetic guidance system

As indicated in Section 4.1, a large axial magnetic field of approximately 0.81- 0.82 T & 4.30 T is required for the operation of gyrotrons. This is provided by a super conducting NbTi solenoid. The magnet has a 12.5 cm. mean radius and is

capable of producing a maximum magnetic field of 0.814 T with a field inhomogeneity of approximately 1 percent for 42 GHz. (Interestingly, a certain amount of inhomogeneity is desirable in Gyrotron magnets in order to avoid RF power generation outside of the cavity). For 110GHz, the magnet has a 9.0 cm. mean radius and is capable of producing a maximum magnetic field of 4.30 T.

Table 4.3

Super conducting coil data

Specification	**For 42 GHz**	**For 110 GHz**
Coil length	30.0 cm	30.0 cm
Coil mean radius	12.5 cm	9.0 cm
Coil width	2.0 cm	5.0 cm
Total coil current	30.0 A	60.0 A
Coil current density	4216 A/cm^2	8000 A/cm^2
Number of coil turns	8432	20000
Maximum magnetic field	0.814 T	4.30 T
Bore hole radius	8.0 cm	----

CHAPTER 5 STATIC ELECTROMAGNETIC ANALYSIS

5.1Magnetic guidance system

A simple and cost-effective magnet design is achieved using a single coil, which gives the maximum required field at the center of the cavity and uses the stray field in the gun and collector region. For a super-conducting magnet, the inner radius of the coil should be approximately 4 cm larger than the bore radius to permit sufficient space for insulation. The magnetic field is uniform over the resonator midsection and a compression factor of 11 can be obtained at around 33.5 cm behind the resonator midsection. It is also possible to use a normal (not super conducting) electromagnet. The super conducting coil data for the 42 GHz and 110 GHz gyrotron is given in the Table 5-1.

Table 5-1

Super conducting coil data

Specification	**For 42 GHz**	**For 110 GHz**
Coil length	30.0 cm	30.0 cm
Coil mean radius	12.5 cm	9.0 cm
Coil width	2.0 cm	5.0 cm
Total coil current	30.0 A	60.0 A
Coil current density	4216 A/cm^2	8000 A/cm^2
Number of coil turns	8432	20000
Maximum magnetic field	0.814 T	4.30 T

5.2 ANSYS approach:

(A) 2-Dimensional

The 2-dimensional coil is modeled with the dimensions given in the Table I. A current of required ampere (30A & 60A) is made to flow in the coil and the flux pattern is observed.

(B) 3-Dimensional

The 3-dimensional coil is modeled with the dimensions given in the Table I. A current of required ampere (30A & 60A) is made to flow in the coil and the flux pattern is observed.

Modeling

(A) 2-Dimensional

The coil is modeled in 2-dimensionas an axis symmetry model. A large air (approx. 10 times) surrounding the coil is also modeled in order to allow flux lines to pass.

(B) 3-Dimensional

The coil is modeled in 3-dimension. A large air (approx. 10 times) surrounding the coil is also modeled in order to allow flux lines to pass.

Meshing

The model is meshed with mapped Quad meshing using PLANE53 elements in 2-dimension and hexa (sweep) meshing using SOLID97 in 3-dimension. The mesh density at the coil is more than that at the air. The meshing is done in such a way that optimization between solution time and accuracy of result is achieved.

Boundary conditions

A boundary of flux parallel is applied along the outer boundary lines of the air. The current is applied as current density on the coil area in the Z -direction.

Solution phase

The solution is done using the static analysis. The resultant plots such as flux density, flux lines are observed.

Results of 200 KW, 42 GHz gyrotron super conducting coil

Figure 5-1 ANSYS RESULTS (2D)

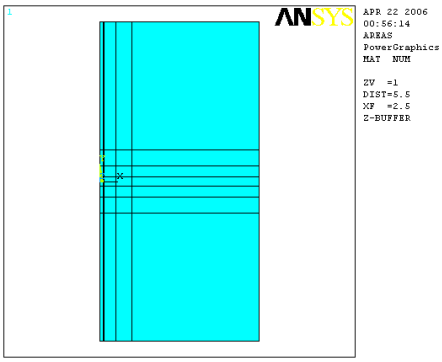

2D Model of air

Dimension: 6m X 6m

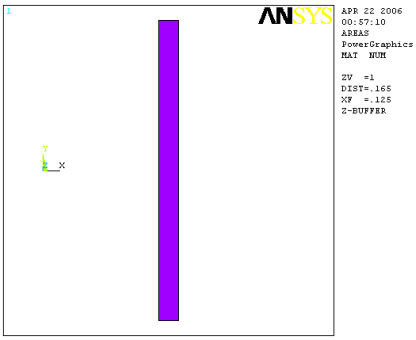

2D Model of coil

Dimension: 0.3m X 0.02m

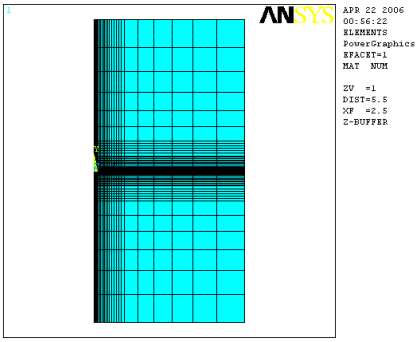

Meshing of model

Dimension: 6m X 6m

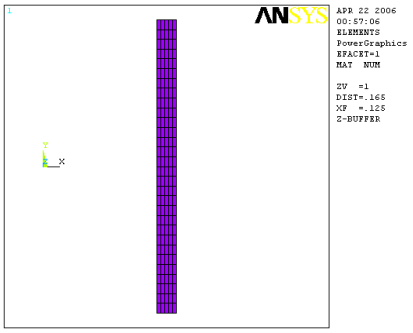

Meshing of coil

Dimension: 0.3m X 0.02m

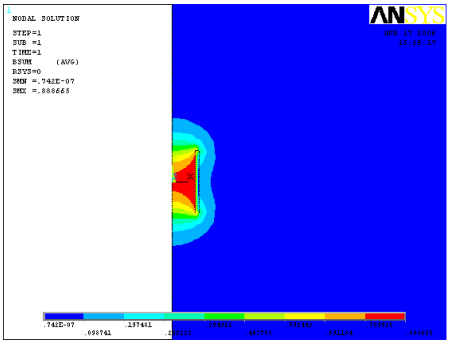

Flux density pattern near the coil

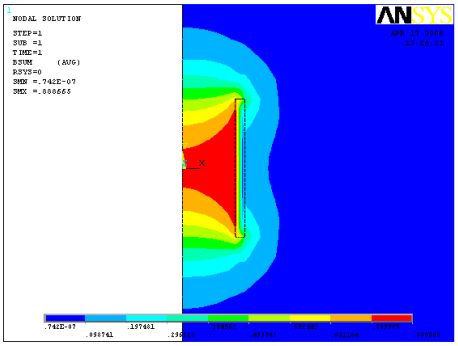

Flux density pattern near the coil

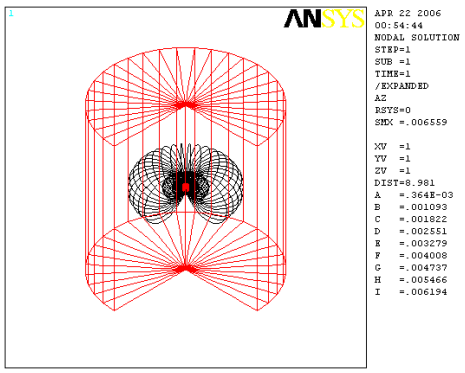

3D Flux lines expanded view

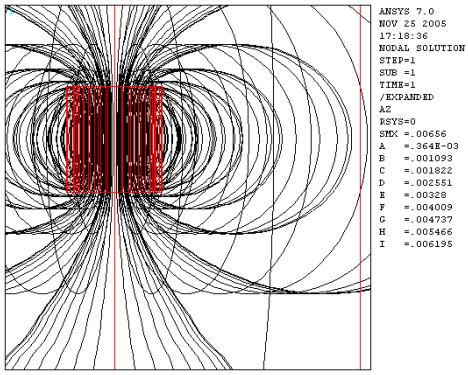

3D Flux lines (zoomed)

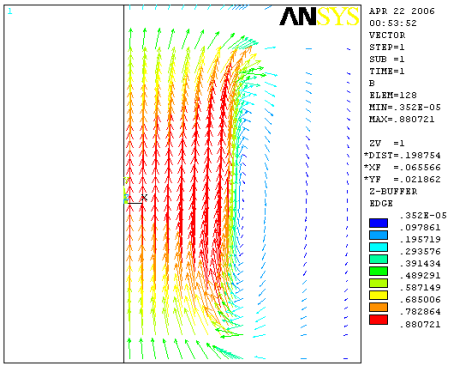

Flux density vector plot near the coil

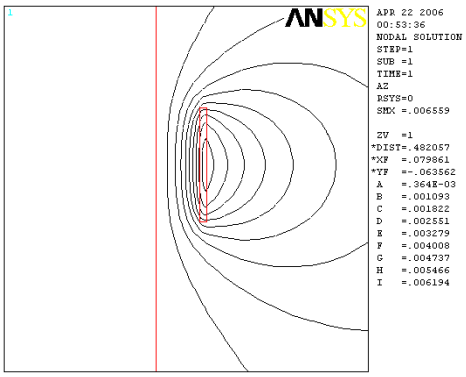

2D Flux lines near the coil

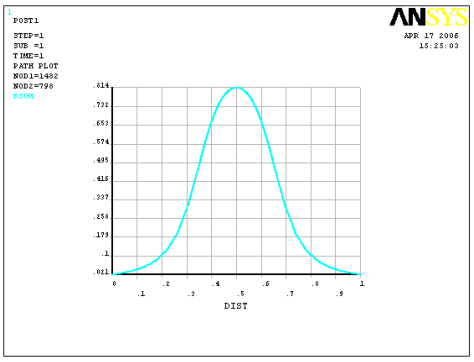

Axial flux density along the center line of the coil

Max. value = 0.814 T

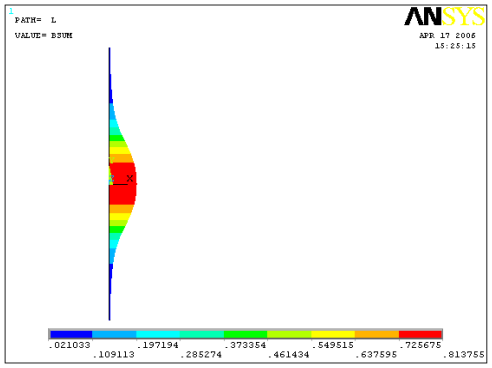

Axial flux density along the center line of the Coil

Max. value = 0.814 T

Figure 5-2 ANSYS RESULTS (3D)

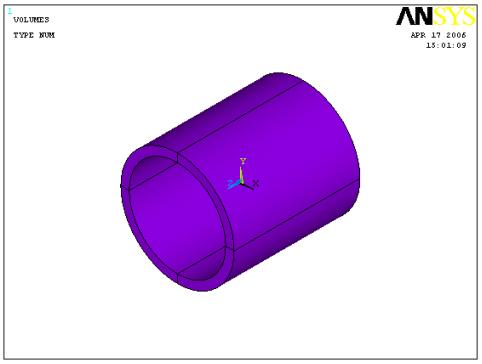

Model of coil

Cross sectional area: 0.3m X 0.02m

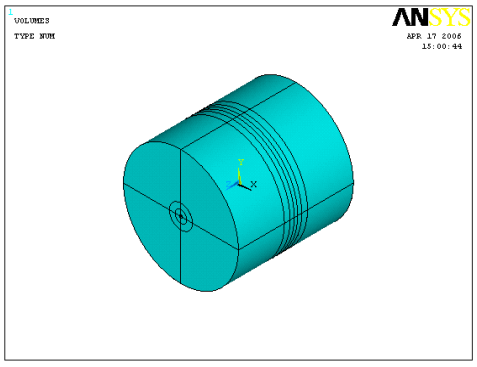

Model of air

Dimensions of cylinder:

Radius = 6m, Height = 6m

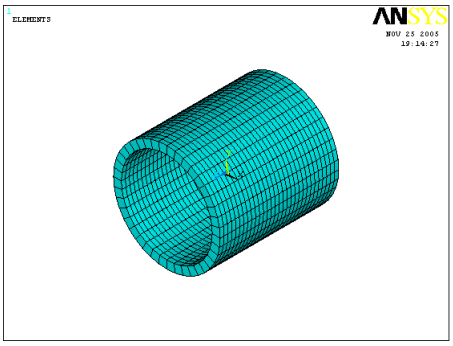

Meshing of coil

Cross sectional area: 0.3m X 0.02m

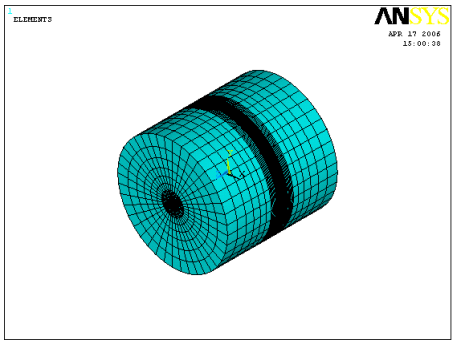

Meshing of air

Dimensions of cylinder:

Radius = 6m, Height = 6m

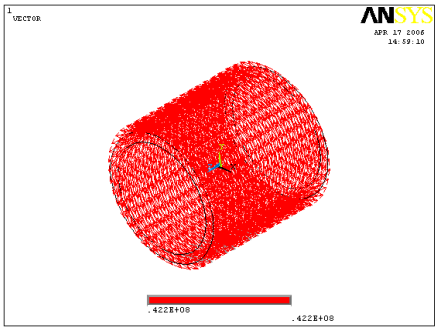

Vector plot of current density in coil

Current density = 4216 A/cm2

Current = 30 A

(*Iso. view*)

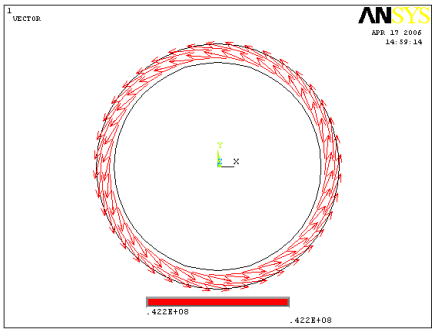

Vector plot of current density in coil

Current density = 4216 A/cm2

Current = 30 A

(*Front view*)

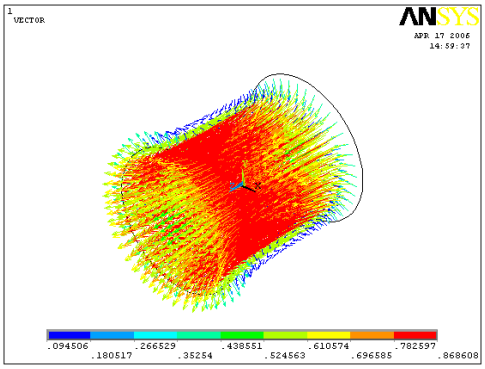

Vector plot of flux density in the coil

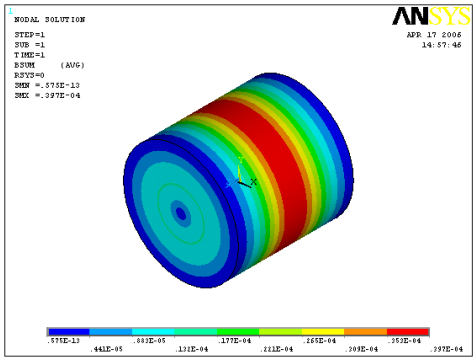

Nodal flux density in the model

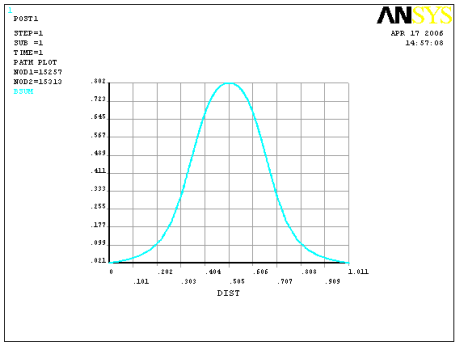

Axial flux density along the center line of the coil

Max. value = 0.802 T

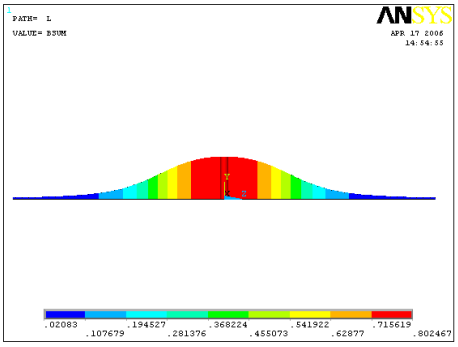

Axial flux density along the center line of the coil

Max. value = 0.802 T

Results of 1 MW, 110 GHz gyrotron super conducting coil

Figure 5-3 ANSYS RESULTS (2D)

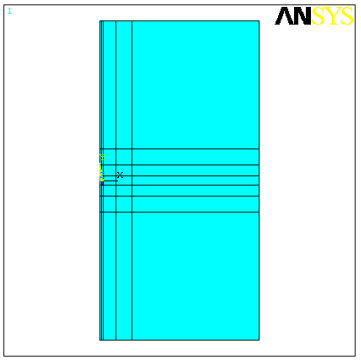

2D Model of air

Dimension: 6m X 6m

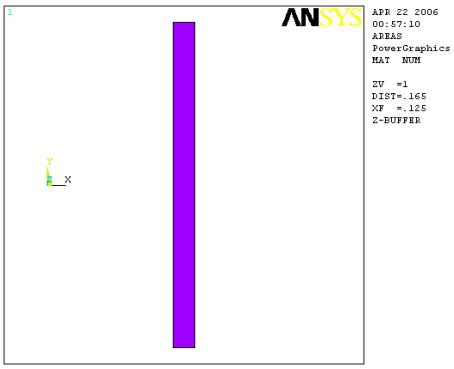

2D Model of coil

Dimension: 0.3m X 0.05m

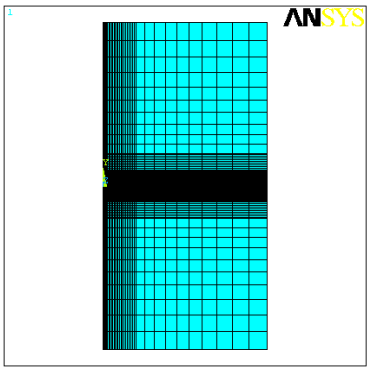

Meshing of model

Dimension: 6m X 6m

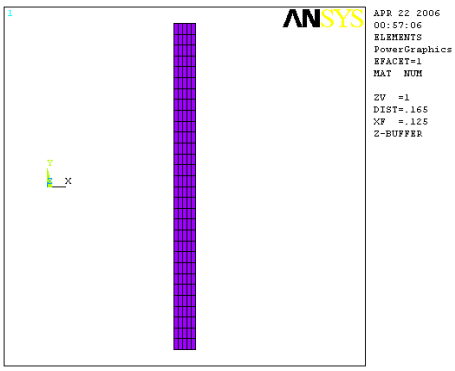

Meshing of coil

Dimension: 0.3m X 0.05m

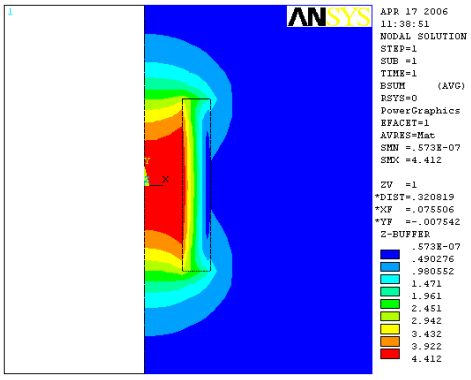

Flux density pattern near the coil

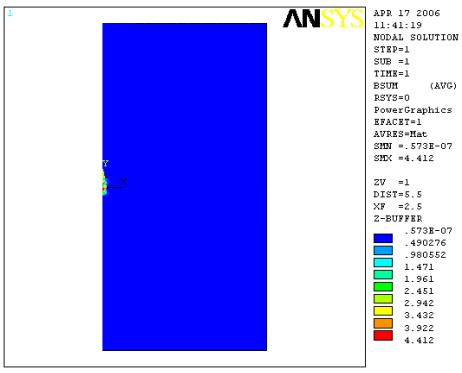

Flux density pattern in the model

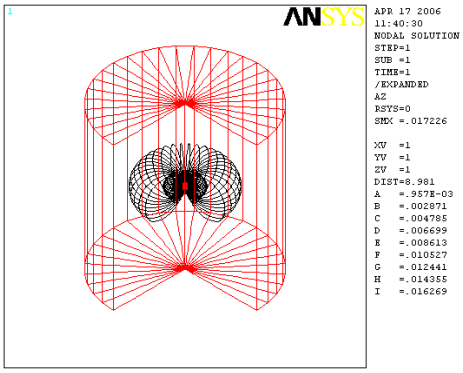

3D Flux lines expanded view

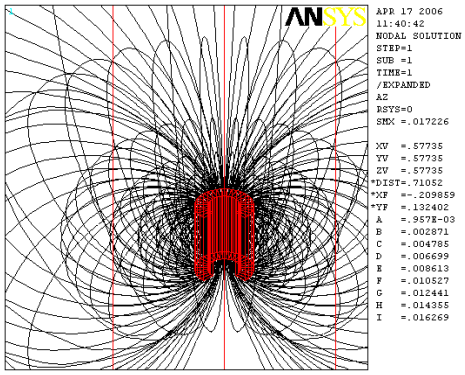

3D Flux lines (zoomed)

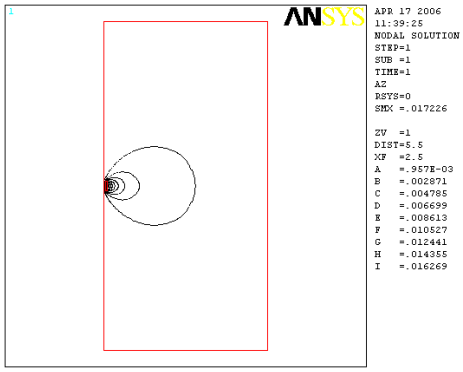

2D Flux lines in the model

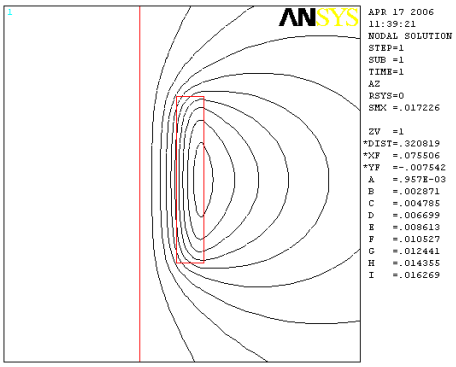

2D Flux lines near the coil

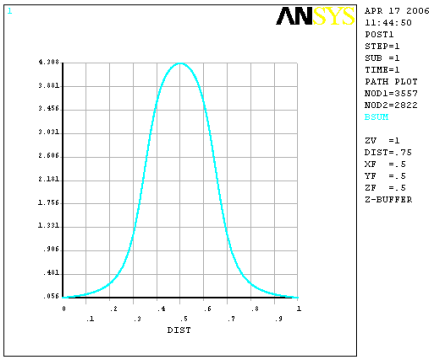

Axial flux density along the center line of the coil

Max. value = 4.308 T

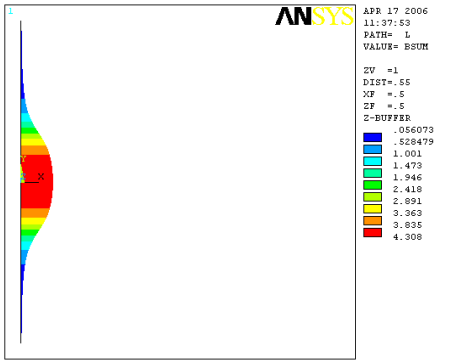

Axial flux density along the center line of the coil

Max. value = 4.308 T

Figure 5-4 ANSYS RESULTS (3D)

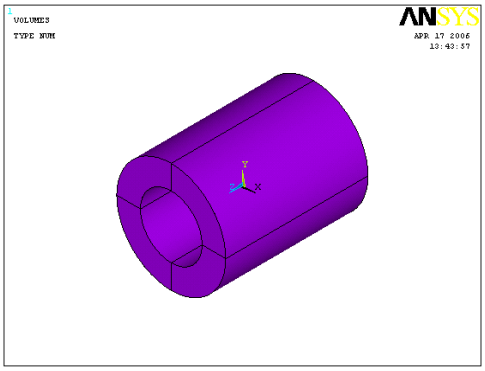

Model of coil

Cross sectional area: 0.3m X 0.05m

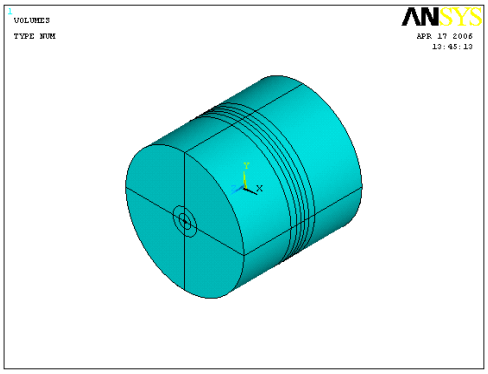

Model of air

Dimensions of cylinder:

Radius = 6m, Height = 6m

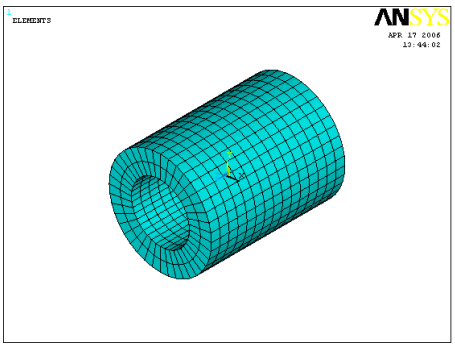

Meshing of coil

Cross sectional area: 0.3m X 0.05m

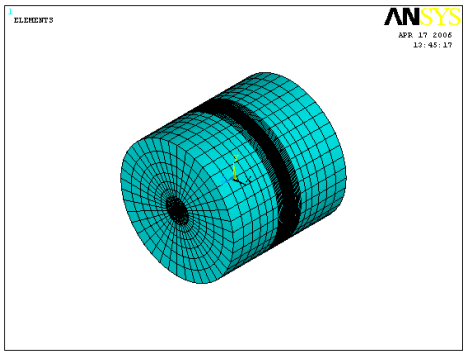

Meshing of air

Dimensions of cylinder:

Radius = 6m, Height = 6m

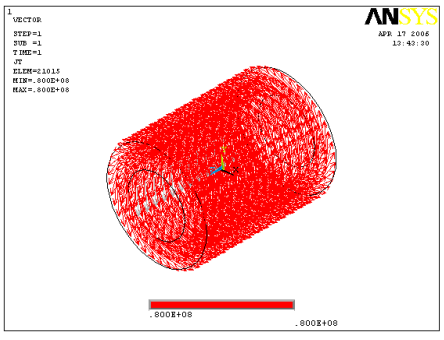

Vector plot of current density in coil

Current density = 8000 A/cm2

Current = 60 A

(*Iso. view*)

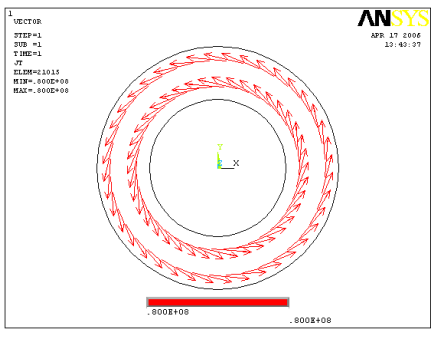

Vector plot of current density in coil

Current density = 8000 A/cm2

Current = 60 A

(*Front view*)

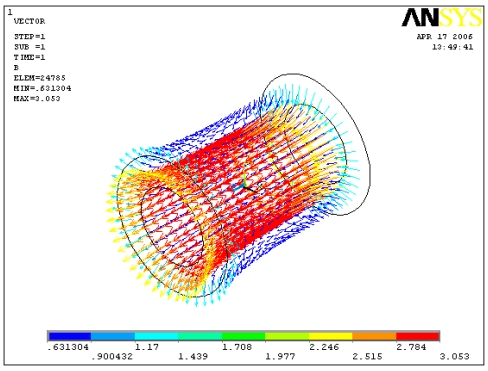

Vector plot of flux density in coil

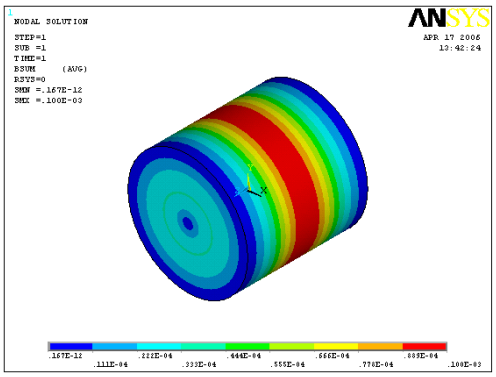

Nodal flux density of model

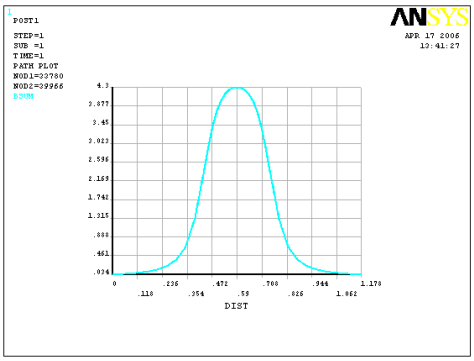

Axial flux density along the center line of the coil

Max. value = 4.3 T

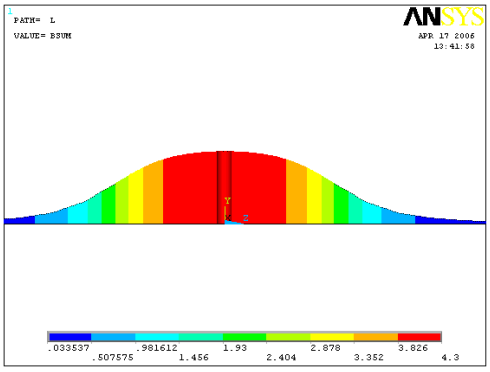

Axial flux density along the center line of the coil

Max. value = 4.3 T

CHAPTER 6 HIGH FREQUENCY MODAL ANALYSIS

6.1 Cavity

The cavity is a standard three-section structure with an input taper and a uniform midsection followed by an output up taper. The beam–wave interaction takes place in the uniform midsection where the RF fields reach peak values.

Table 6-1

CAVITY DATA

Specification	**For 42 GHz**	**For 110 GHz**
Mode	TE_{42}	$TE_{28\,8}$
Frequency (GHz)	42	110
Magnetic field (T)	0.814 T	4.3 T
Diffractive Q	1131	992
Cavity radius (mm)	10.55	26.09
Input taper L_1 (mm),θ_1(°)	45, 2.5°	24, 2.5°
Uniform midsection L_2 (mm),θ_2(°)	50, 0°	19, 0°
Output taper L_3 (mm),θ_3(°)	45,3.5°	24, 3.5°

The up taper with a nonlinear contour connects the cavity with the output waveguide and launcher of the output coupler. Parabolic smoothing of the taper transitions of the cavity walls is performed in order to minimize unwanted mode conversion at sharp transitions. Rounding of length 10 mm was included at each transition. The cavity data is give in Table 6-1

6.2ANSYS approach

Modeling

The cavity is modeled in 3-dimension. The rounding at the transitions is approximated. The ¼ rth model of the cavity is modeled by taking the advantage of symmetry. The material properties used for cavity are $\mu_r = 1, \varepsilon_r = 1$.

Meshing

The model is meshed with Hexa sweep meshing using HF120 elements. The meshing is done in such a way that optimization between solution time and accuracy of result is achieved.

Boundary condition

In case of a modal analysis, i.e. in the study of the eigen modes of structure, there are no external loads or excitations, and the only possible boundary conditions are: A boundary of electric wall is applied at the cavity vacuum and outer copper wall interface. A surface resistance R_s of copper depending upon the resonant frequency of operation is applied as a impedance boundary condition at the cavity vacuum and outer copper wall interface. Impedance boundary condition has to be applied in order to find out the surface losses of the cavity.

$$R_s = \sqrt{\frac{\mu_o \omega}{2\sigma_e}}$$

Where $\mu_o = 4\pi \times 10^{-7}$ H/m

ω = Resonant frequency

σ_e = Conductivity of copper (0.58 X 10^8 S/m)

A default magnetic wall is applied at the symmetry planes.

Solution phase

The solution is done using the modal analysis. As a solution options the frequency range must be defined. It is important to specify that the number of modes need to be extracted, the frequency range, and the calculation of element results. By doing so it is possible to have a result, not only the frequencies of the eigen modes, but also the nodal and element solution for E and H fields.

6.3 Flow chart for performing high frequency modal analysis

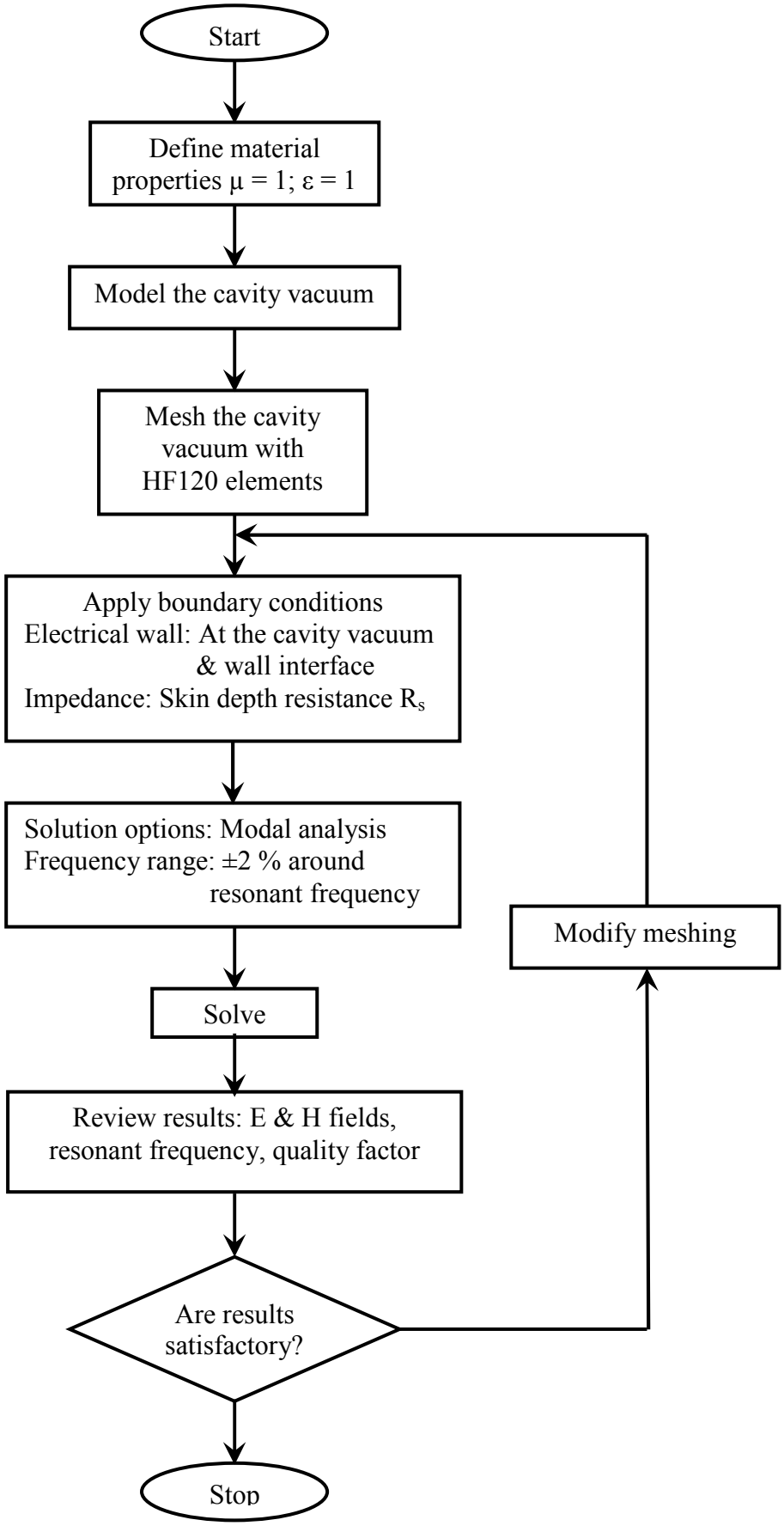

Results of 200 KW, 42 GHz gyrotron cavity

Figure 6-1 ANSYS RESULTS (High frequency)

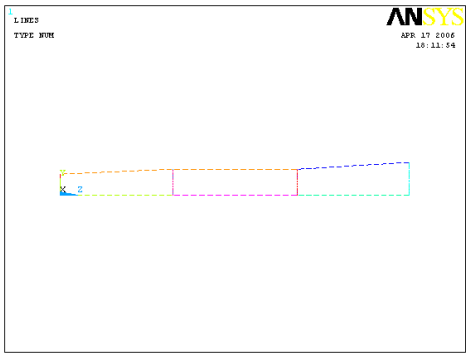

Model of the cavity (*Side view*)

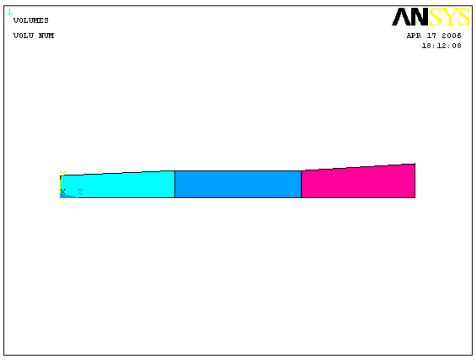

Solid model of the cavity (*Side view*)

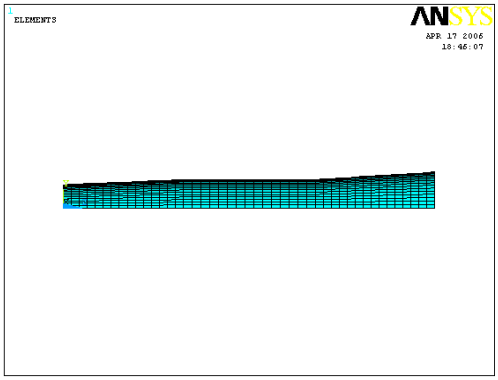

Meshing of the cavity (*Side view*)

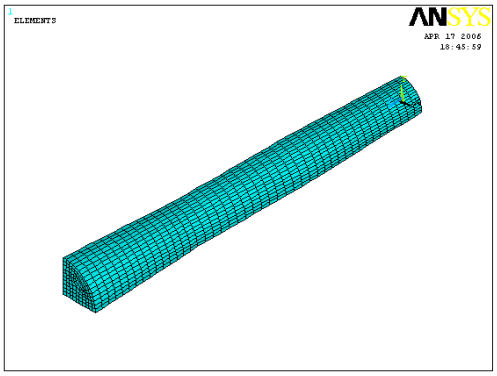

Meshing of the cavity (*Iso. view*)

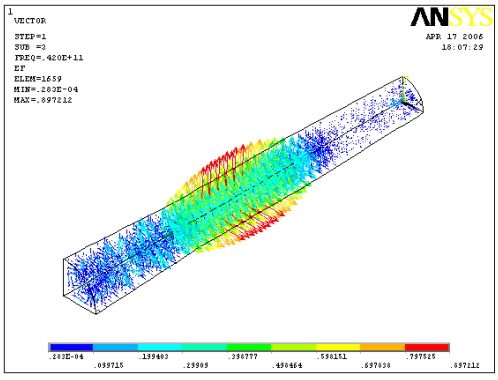

Vector plot of electric field

Mode TE_{42} (*Iso. view*)

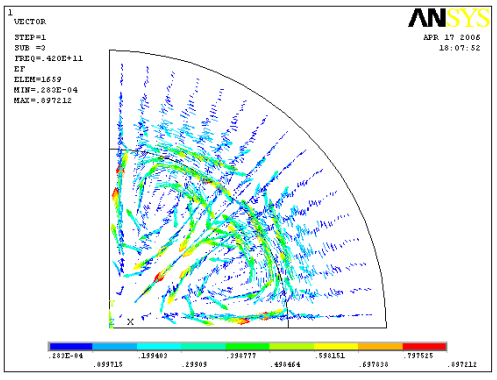

Vector plot of electric field

Mode TE_{42} (*Front view*)

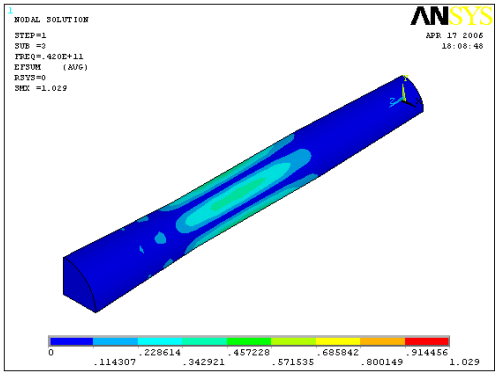

Nodal plot of electric field

Max = 1.029; Min = 0 (*Iso. view*)

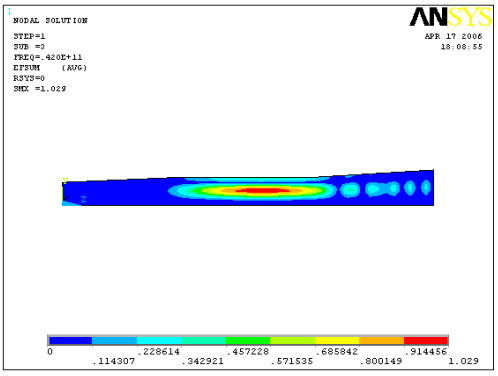

Nodal plot of electric field

Max = 1.029; Min = 0 (*Side view*)

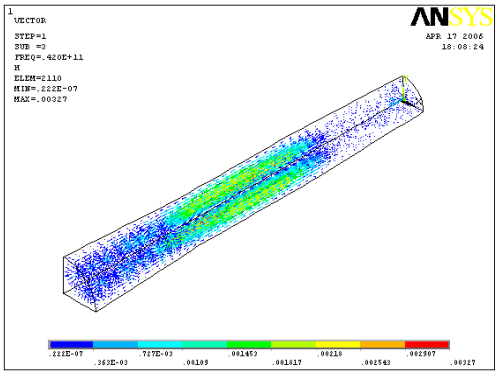

Vector plot of magnetic field

Mode TE_{42} (*Iso. view*)

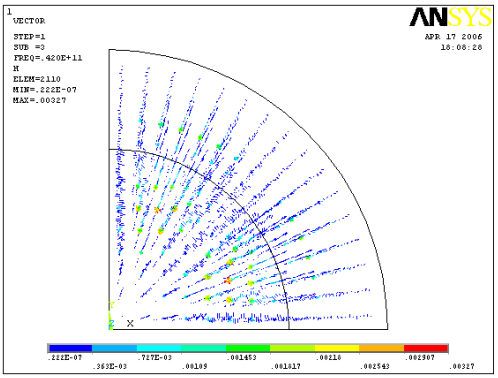

Vector plot of magnetic field

Mode TE_{42} (*Front view*)

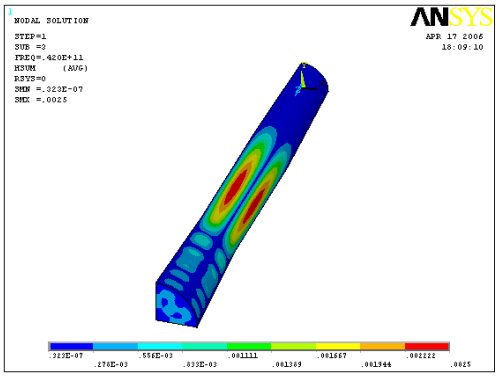

Nodal plot of magnetic field

Max = .0025; Min = 0 (*Iso. view*)

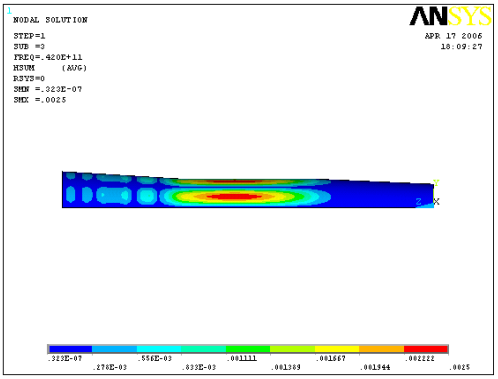

Nodal plot of magnetic field

Max = .0025; Min = 0 (*Iso. view*)

Figure 6-2 ANSYS RESULTS (Thermal[1])

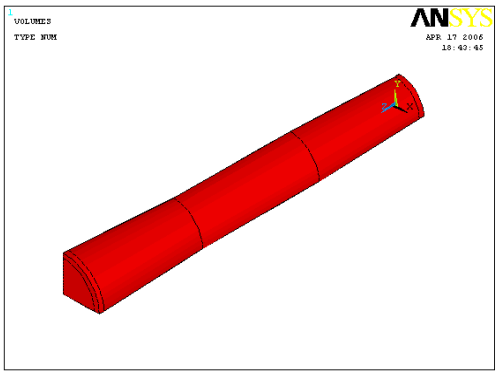

Model of cavity wall (*Iso. view*)

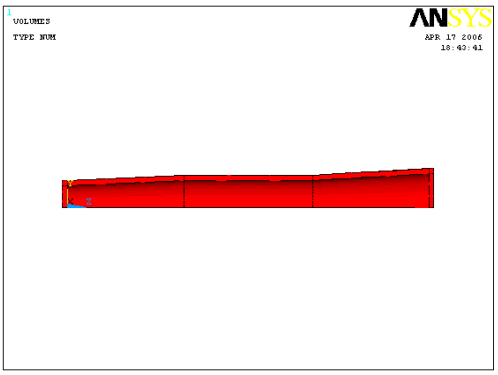

Model of cavity wall (*Side view*)

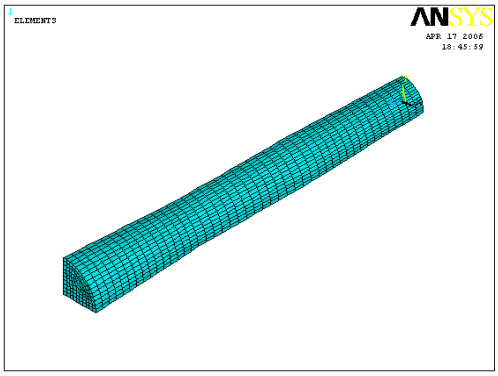

Meshing of cavity wall (*Iso. view*)

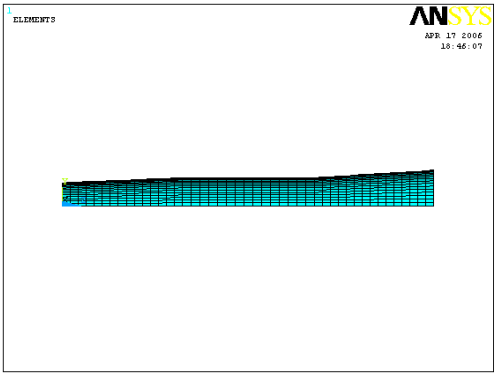

Meshing of cavity wall (*Side view*)

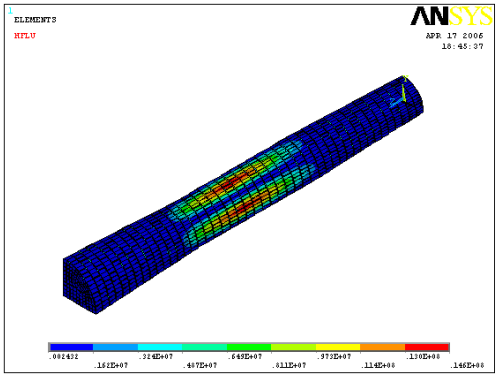

Heat flux at outer surface of cavity vacuum (*Iso. view*)

Max = 14.6 X 10^{10}; Min = 0

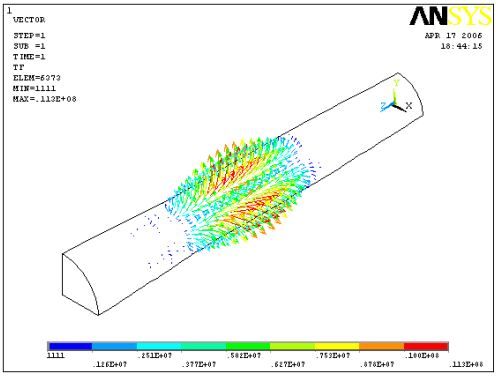

Thermal flux in the cavity copper wall (*Side view*)

Max = 11.3 X 10^{10}; Min = 11.1 X 10^{2}

Thermal[1]: The procedure to perform thermal analysis is explained in the chapter 7.

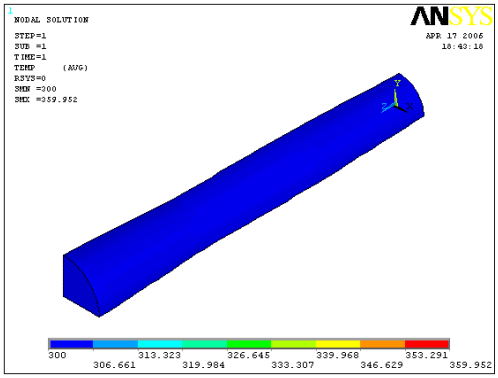

Temperature distribution on the cavity copper wall (*Iso. view*)
Max = ~360^{0}K; Min = 300^{0}K

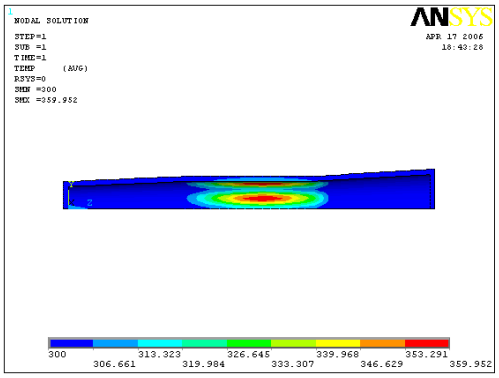

Temperature distribution on the cavity copper wall (*Side view*)
Max = ~360^{0}K; Min = 300^{0}K

Results of CW 1 MW, 110 GHz gyrotron cavity

Figure 6-3 ANSYS RESULTS (High frequency)

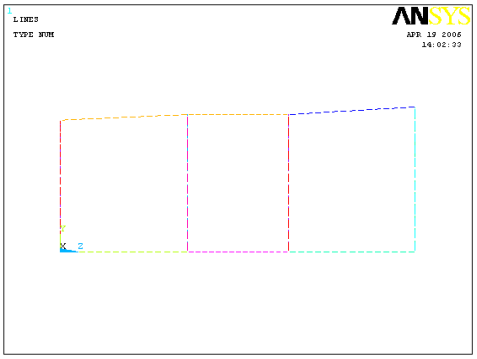

Model of the cavity (*Side view*)

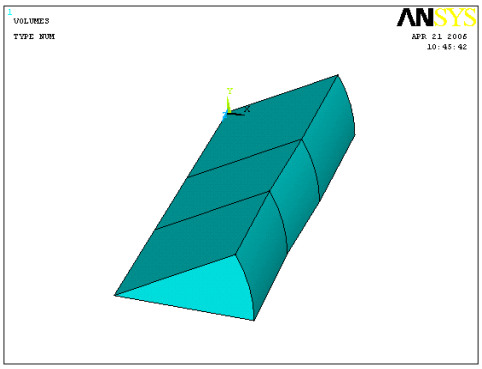

Solid model of the cavity (*Iso. view*)

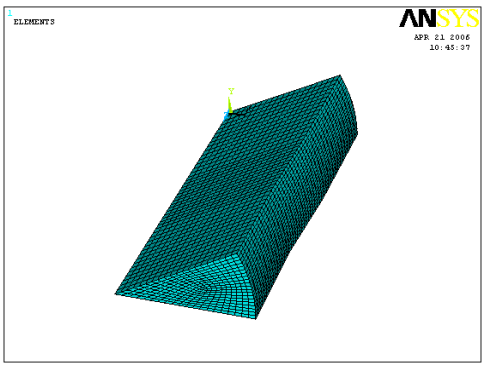

Meshing of the cavity (*Side view*)

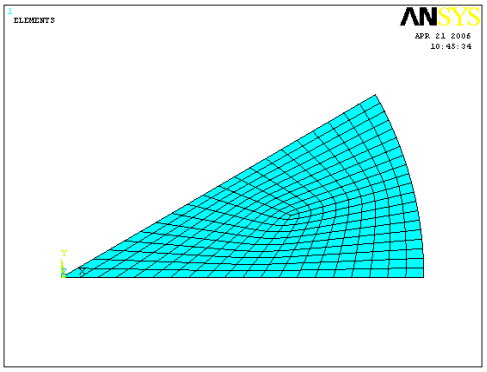

Meshing of the cavity (*Front view*)

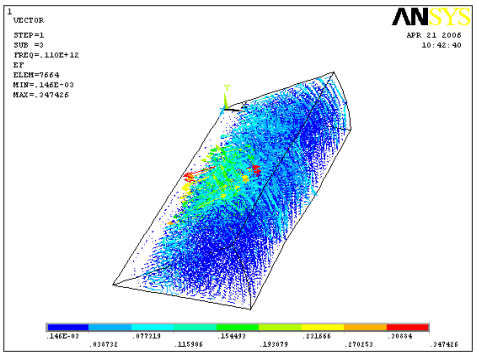

Vector plot of electric field

Mode $TE_{28\,8}$ (*Iso. view*)

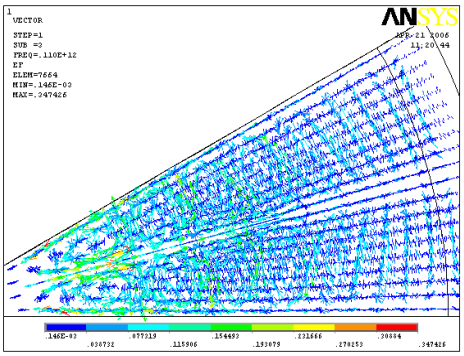

Vector plot of electric field

Mode $TE_{28\,8}$ (*Front view*)

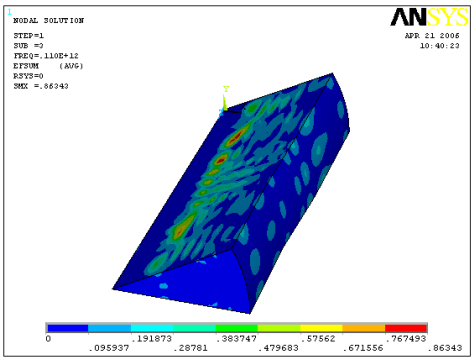

Nodal plot of electric field

Max = .8634; Min = 0 (*Iso. view*)

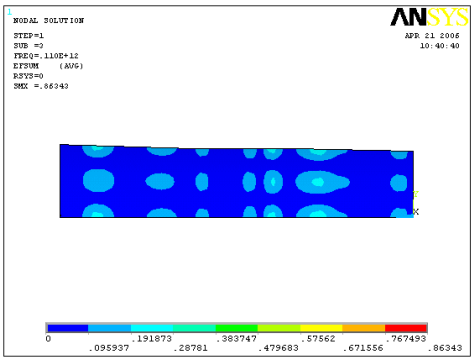

Nodal plot of electric field

Max = .8634; Min = 0 (*Side view*)

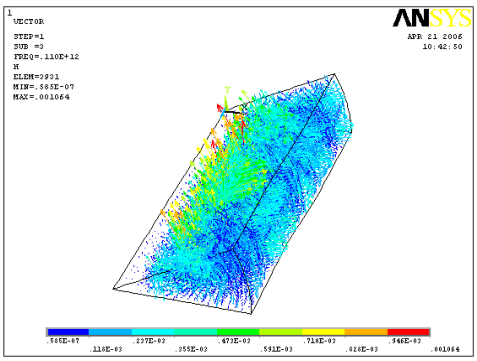

Vector plot of magnetic field

Mode $TE_{28\,8}$ (*Iso. view*)

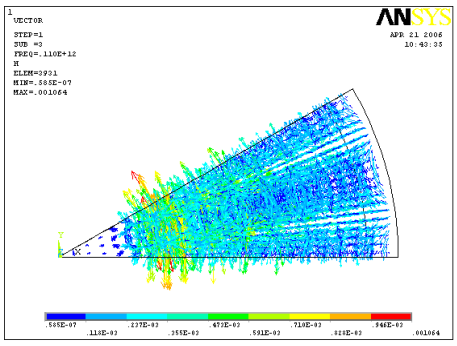

Vector plot of magnetic field

Mode $TE_{28\,8}$ (*Front view*)

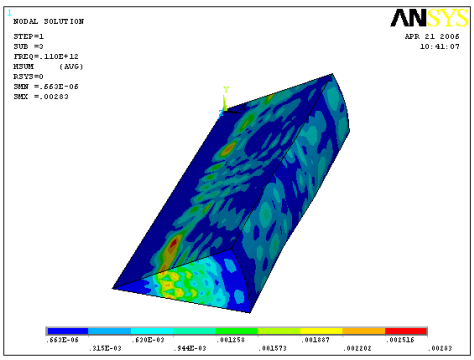

Nodal plot of magnetic field

Max = .00283; Min = 0 (*Iso. view*)

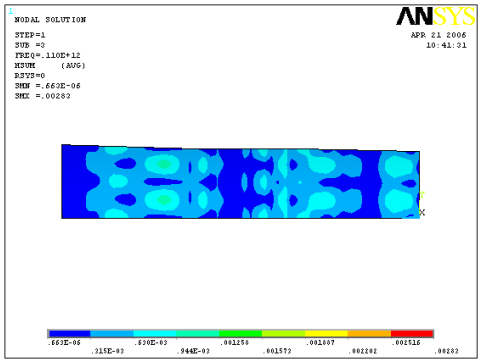

Nodal plot of magnetic field

Max = .00283; Min = 0 (*Iso. view*)

Figure 6-4 ANSYS RESULTS (Thermal[2])

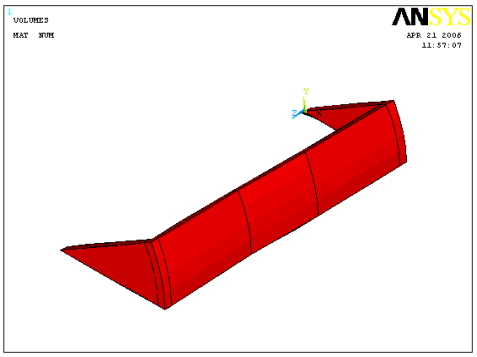

Solid model of cavity wall

(*Iso. view*)

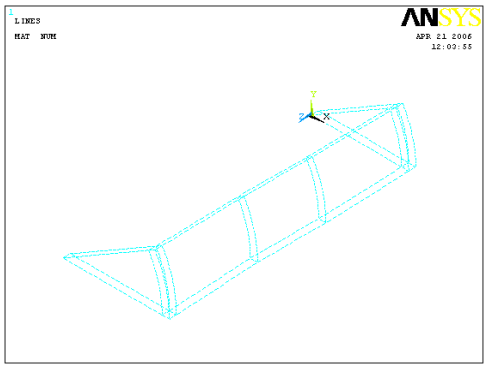

Line model of cavity wall

(*Iso. view*)

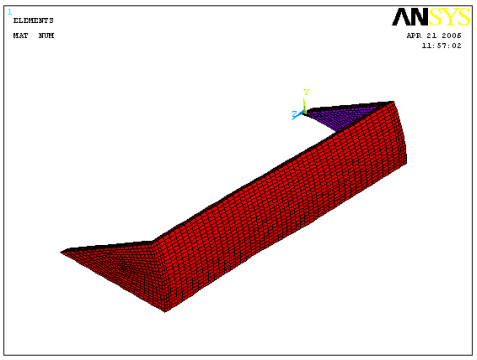

Meshing of cavity wall

(*Iso. view*)

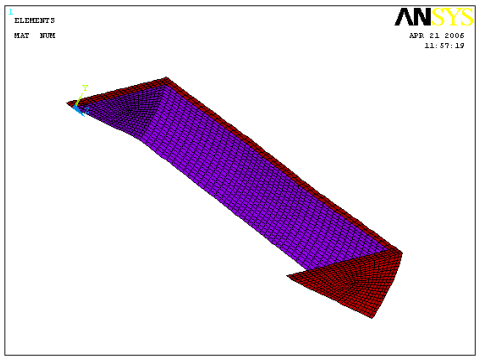

Meshing of cavity copper wall

Thermal[2]: The procedure to perform thermal analysis is explained in the chapter 7.

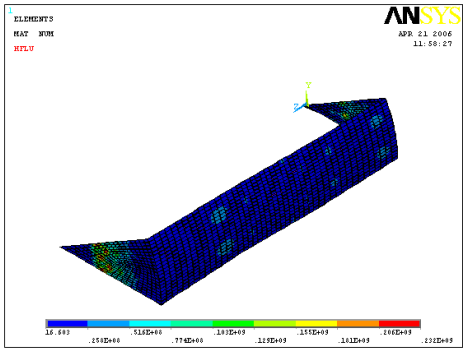

Heat flux at the outer surface of cavity vacuum (*Iso. view*)

Max = 2.32 X 10^{10}; Min = 1.66 X 10^{1}

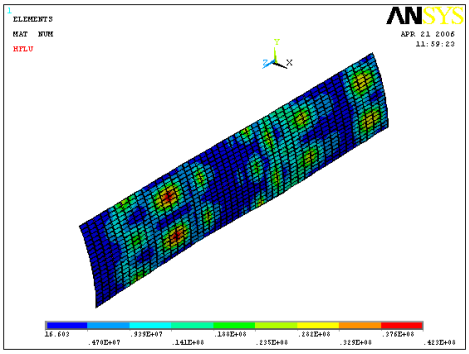

Heat flux at the outer surface of cavity vacuum (*Iso. view*)

Max = 0.423 X 10^{10}; Min = 1.6 X 10^{1}

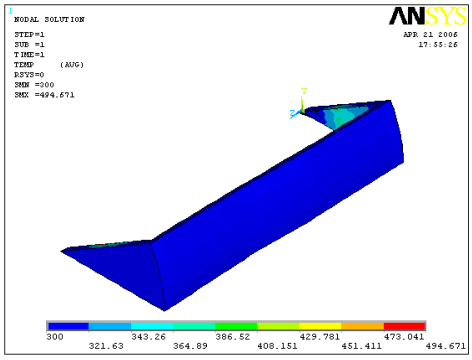

Temperature distribution on the cavity copper wall (*Iso. view*)

Max = ~495^{0}K; Min = 300^{0}K

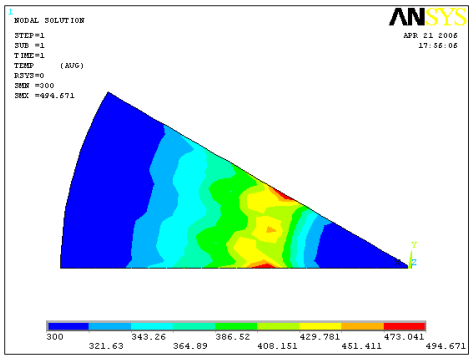

Temperature distribution on the cavity copper wall (*Front view*)

Max = ~495^{0}K; Min = 300^{0}K

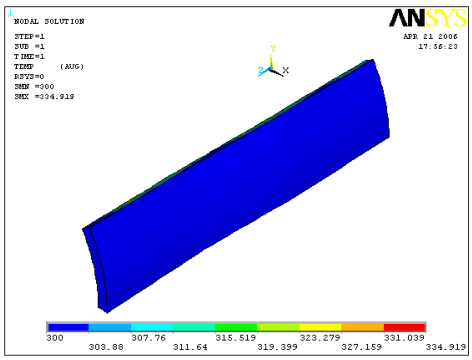

Temperature distribution on the cavity side copper wall (*Iso. view*)

Max = ~335^{0}K; Min = 300^{0}K

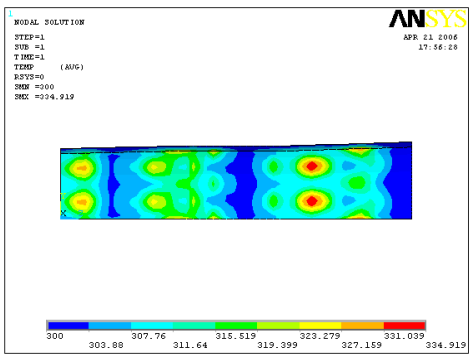

Temperature distribution on the cavity side copper wall (*Front view*)

Max = ~335^{0}K; Min = 300^{0}K

7.1 500 MHz Pillbox cavity data

Table 7-1

PILLBOX CAVITY DATA

Specification	**For 500 MHz**
Mode	TM_{010}
Frequency (GHz)	0.5
Unloaded quality factor Q_0	13896.40
Cavity radius (m)	0.22966
Cavity length L (m)	0.05
Peak power density (w/cm^2)	2.78

Analysis methodology to perform the coupled-field analysis:

Modal analysis:

- Model the cavity vacuum volume for performing the high frequency modal analysis.
- Model run time is reduced by taking advantage of cavity symmetry.
- Material properties applied for the cavity vacuum are $\mu_r = 1, \varepsilon_r = 1$.
- Vacuum volume is meshed with brick RF elements (HF120) with a finer mesh at the critical areas.
- Electric wall and impedance boundary (surface resistance R_s = 5.834E-3 Ω due to skin depth for 500 MHz) conditions are applied to the exterior surfaces of the cavity vacuum representing the cavity wall-to-vacuum interfaces.
- Model symmetry planes default to magnetic wall boundary condition.
- A modal RF analysis is run resulting in calculation of the cavity frequency and Q as well as normalized data for the E and H fields.

Thermal analysis:

- The initial step in developing the thermal model is to generate a new surface mesh on the cavity surface that matches node-for-node the mesh on the surface of the RF model.

- The new mesh consists of surface elements (SURF152) without mid-side nodes (key opt. 4 = 1) and with heat flux loading capability (key opt. 8 = 1).
- Next, a macro consisting of an input file with a sequential list of ANSYS commands reads in the H (magnetic) field at each surface node of the RF elements (HF120).
- The total cavity wall heat flux is found by the value ½•R_s•H^2 •dA over all the surface nodes – R_s: Surface Resistance due to skin depth, H: normalized magnetic field, dA: based on the element areas adjacent to nodes.
- The results are scaled based on the known total heat loss in the cavity and applied to the new surface elements (SURF152) as a load. Due to the normalized data of the magnetic field scaling has to be done.
- Thermal analysis begins by deleting the RF loads, RF elements (HF120) and associated volume(s), leaving only the new surface elements (SURF152) with applied heat fluxes.
- Build the thermal solid model of the cavity around the existing cavity surface areas; be sure to duplicate the areas that are meshed with surface elements (SURF152) because the new volume can't use areas that are meshed.
- After the modeling of cavity wall volume has been completed, merge keypoints to attach the area containing the heat flux elements (SURF152) to the new volume.
- Apply thermal material properties for the cavity wall (thermal conductivity).
- Meshed the model with thermal elements (SOLID90), and apply boundary conditions (uniform temperature of 300^oK at the exterior surface of the copper wall; in this case) and solve for static thermal analysis.
- Observe the temperature distribution over the cavity copper wall.

Structural analysis:

- To perform the structural analyses change the thermal elements (SOLID90) to structural elements (SOLID95) and material properties also.
- Next the temperature distribution of thermal analysis as load for the structural analysis and applying symmetry boundary conditions on the symmetry planes, fixed-point boundary conditions at the left cavity center to perform the structural analysis.
- Observe the thermal equivalent stress distribution, check whether it is in the elastic limit or not.

7.2 Flow chart for performing coupled-field analysis

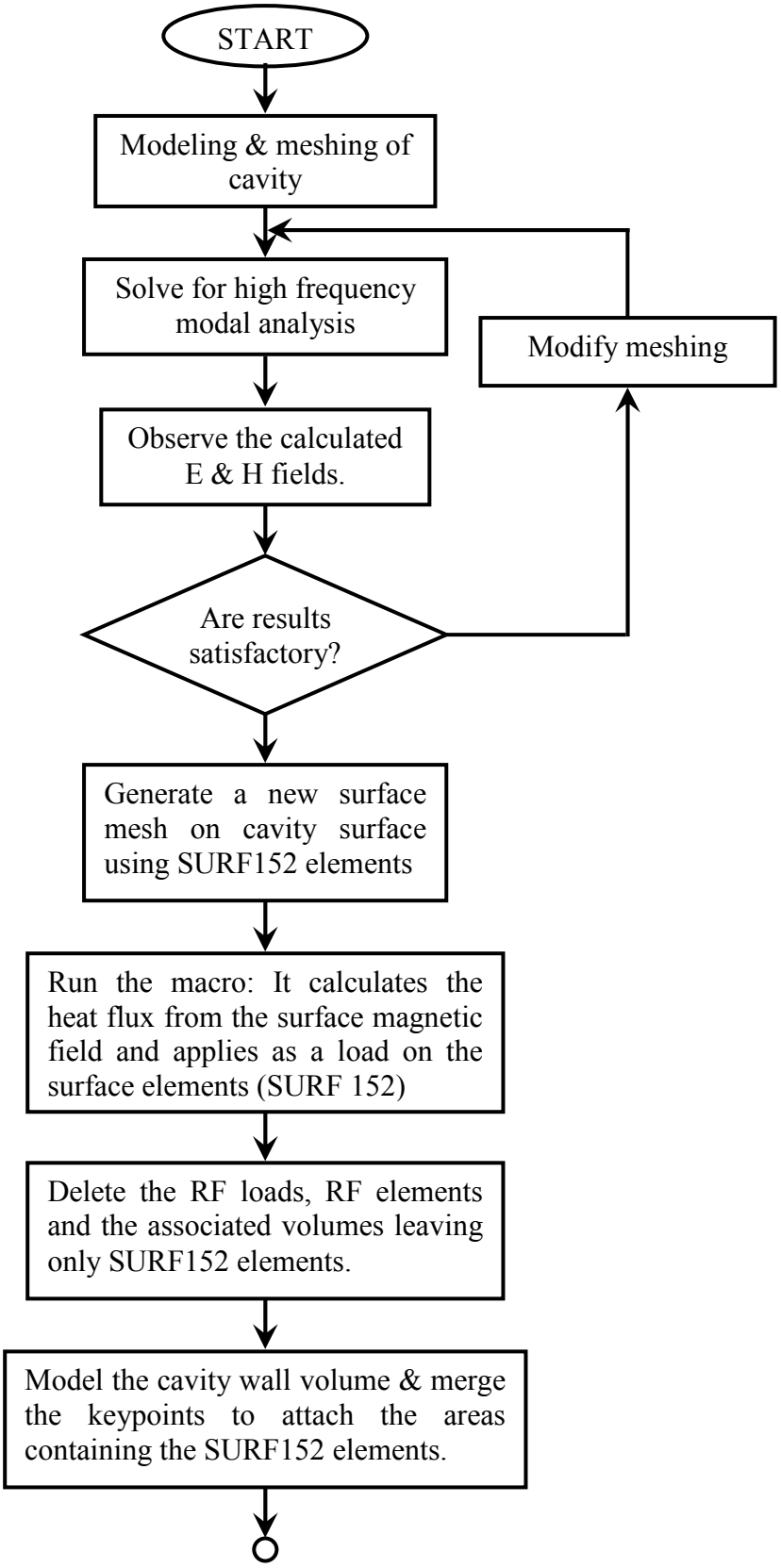

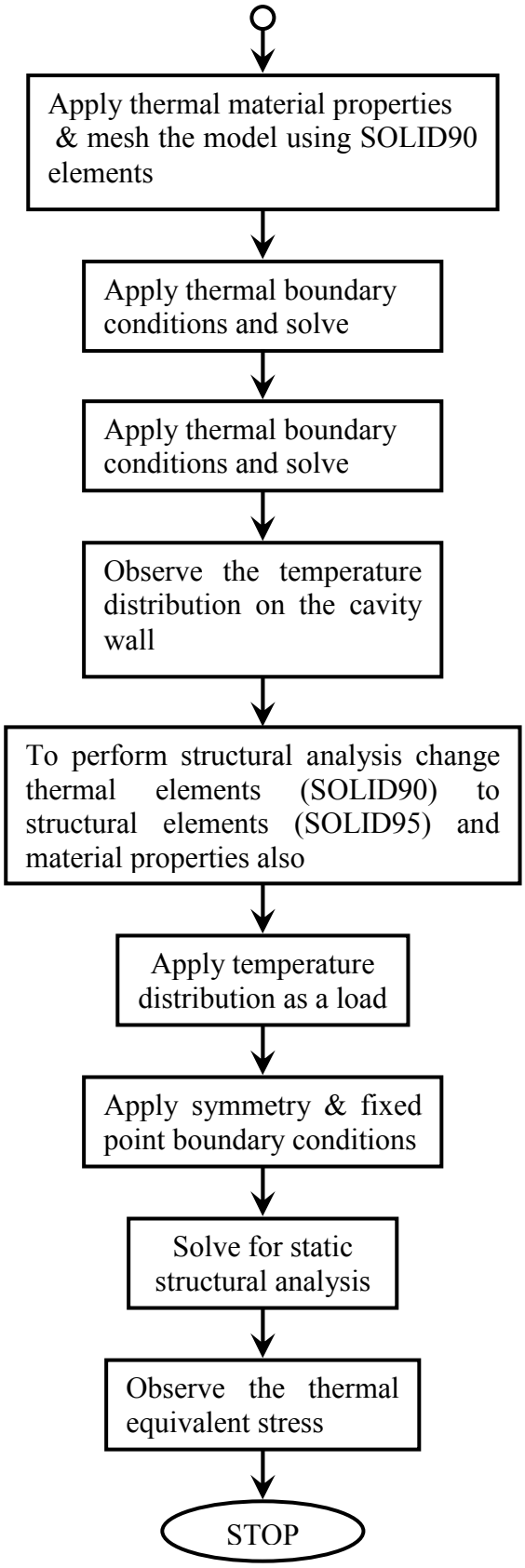
Apply thermal material properties & mesh the model using SOLID90 elements
Apply thermal boundary conditions and solve
Apply thermal boundary conditions and solve
Observe the temperature distribution on the cavity wall
To perform structural analysis change thermal elements (SOLID90) to structural elements (SOLID95) and material properties also
Apply temperature distribution as a load
Apply symmetry & fixed point boundary conditions
Solve for static structural analysis
Observe the thermal equivalent stress
STOP

Results of 500 MHz Pillbox cavity

Figure 7-1 ANSYS RESULTS (High frequency)

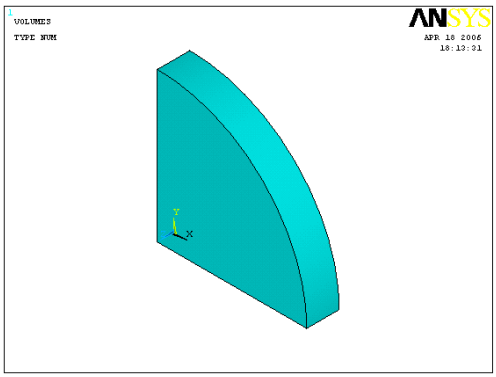

Model of the cavity (*Iso. view*)

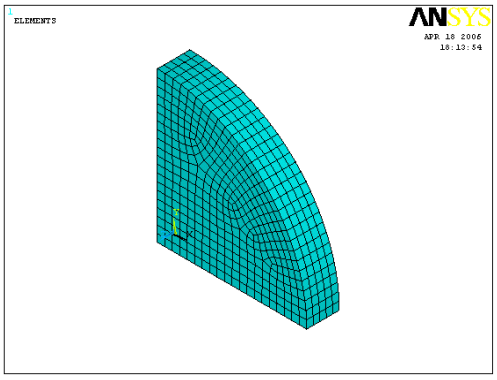

Meshing of the cavity (*Iso. view*)

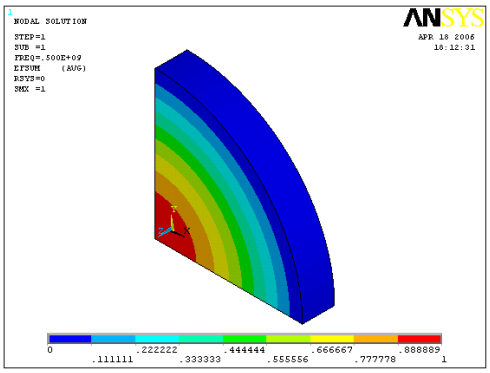

Nodal plot of electric field

Max = 1; Min = 0 (*Iso. view*)

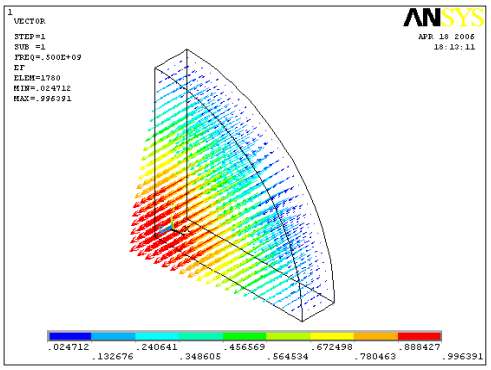

Vector plot of electric field

Mode TM_{010} (*Iso. view*)

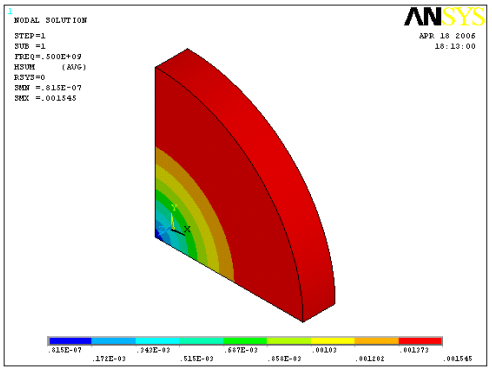

Nodal plot of magnetic field

Max = 0.001545; Min = 0 (*Iso. view*)

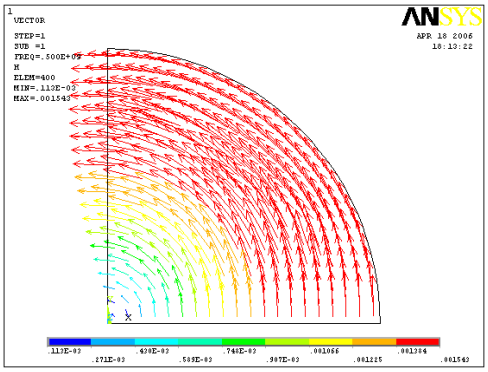

Vector plot of magnetic field

Mode TM_{010} (*Iso. view*)

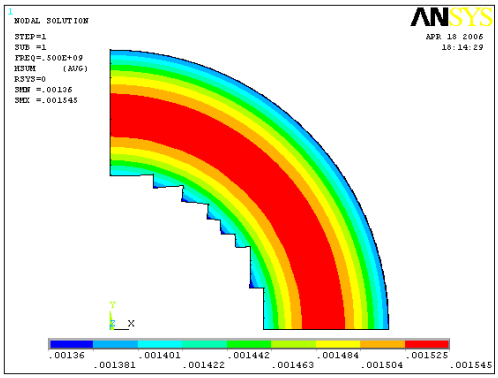

Nodal plot of magnetic field at the top of the cavity (*Front view*)

Max = 0.001545; Min = 0.00136

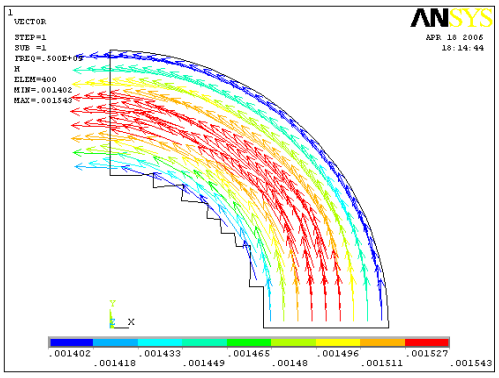

Vector plot of the magnetic field at the top of the cavity (*Front view*)

Max = 0.001545; Min = 0.00136

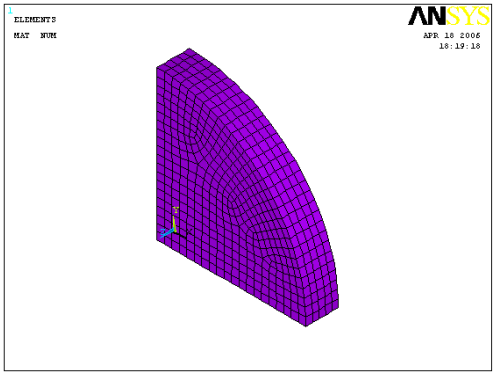

Surface elements at vacuum and wall interface (*Iso. view*)

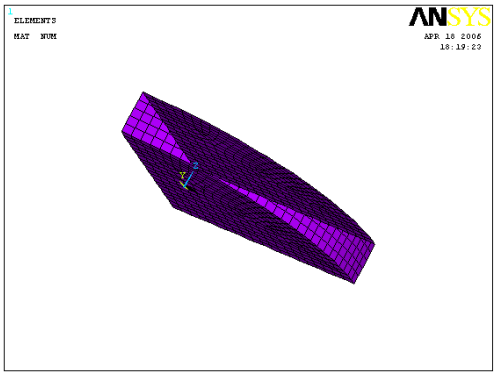

Surface elements at vacuum and wall interface

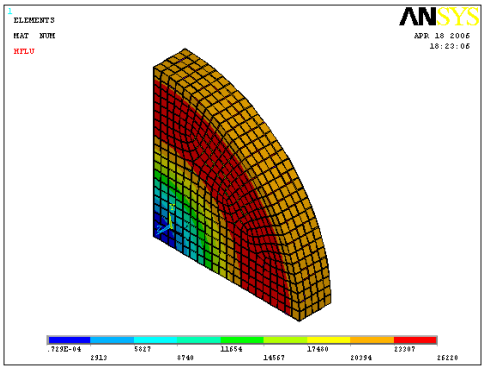

Heat flux on the surface elements (*Iso. view*)

Max = 26220; Min = 0

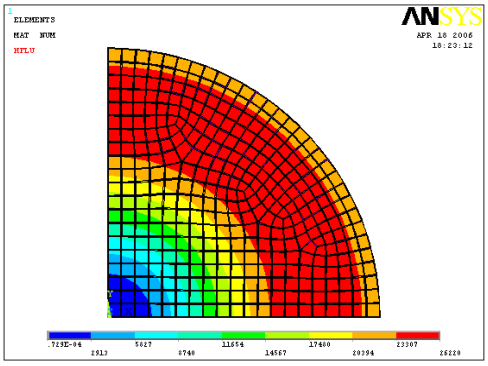

Heat flux on the surface elements (*Front view*)

Max = 26220; Min = 0

Figure 7-2 ANSYS RESULTS (Thermal)

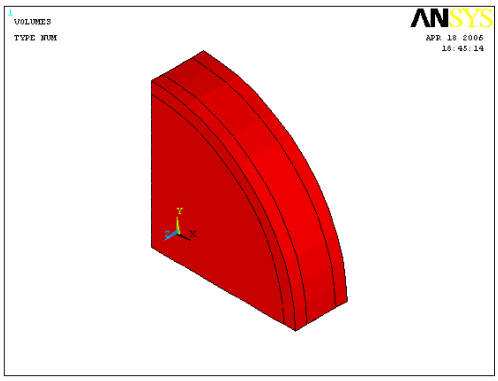

Model of cavity wall (*Iso. view*)

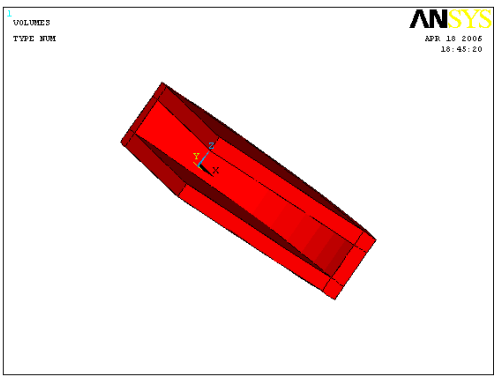

Model of cavity copper wall

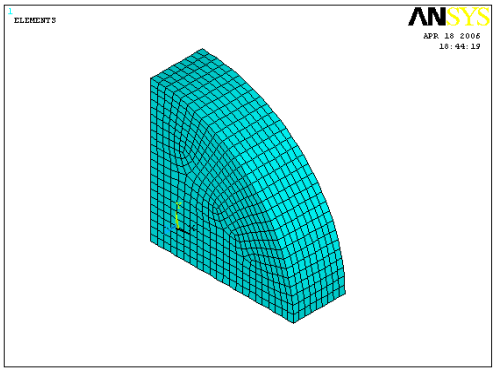

Meshing of the cavity wall (*Iso. view*)

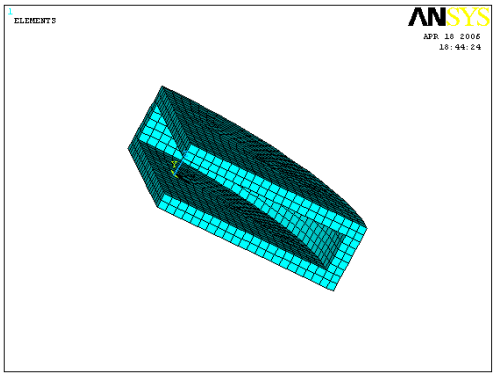

Meshing of the cavity wall

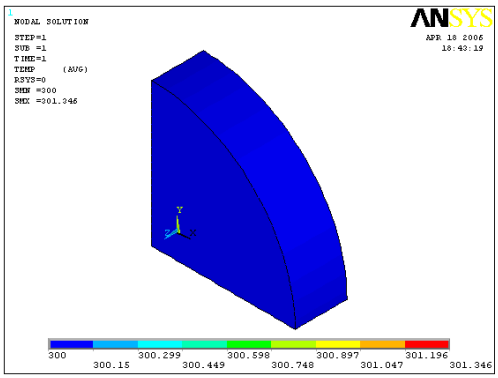

Temperature distribution on the copper wall (*Iso. view*)

Max = 301.346^{0}K; Min = 300^{0}K

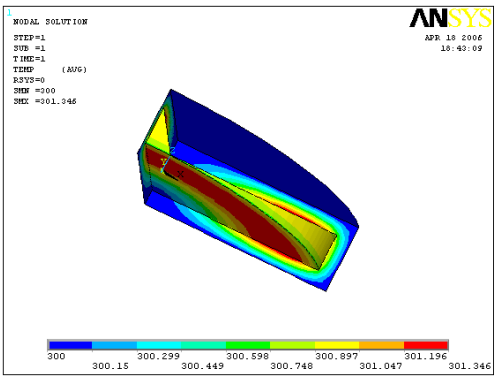

Temperature distribution on the copper wall

Max = 301.346^{0}K; Min = 300^{0}K

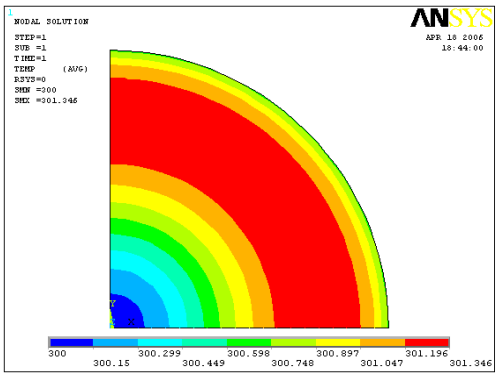

Temperature distribution on the copper wall (*Front view*)

Max = 301.346^{0}K; Min = 300^{0}K

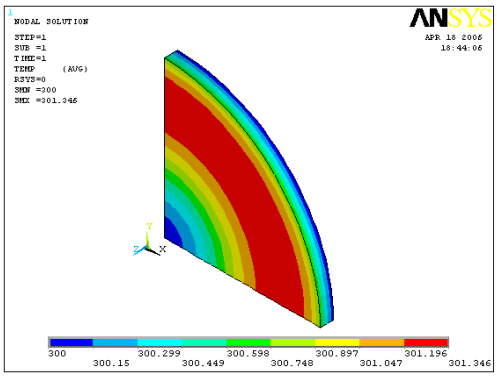

Temperature distribution on the copper wall (*Iso. view*)

Max = 301.346^{0}K; Min = 300^{0}K

Figure 7-3 ANSYS RESULTS (Structural)

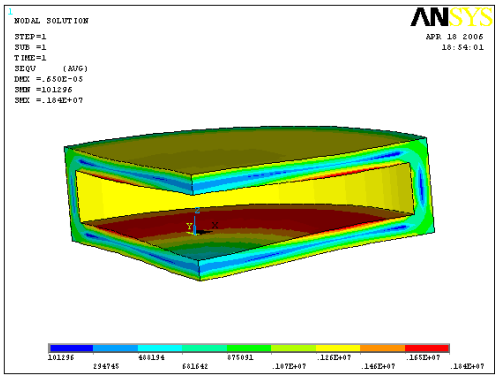

Thermal stress on the cavity walls

Max = 1.84 MPa; Min = 0.1 MPa

Deformation = 6.5 µm

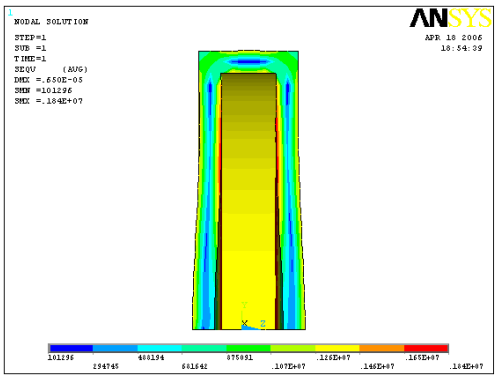

Thermal stress on the cavity walls

Max = 1.84 MPa; Min = 0.1 MPa

Deformation = 6.5 µm

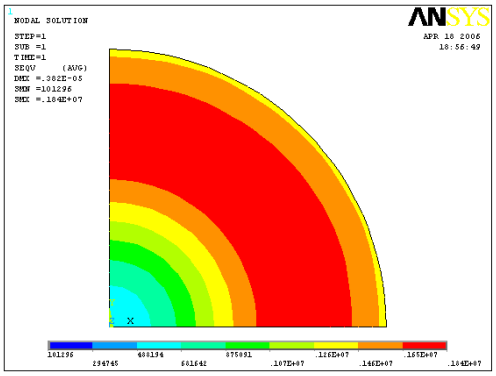

Thermal stress on the cavity wall

Max = 1.84 MPa; Min = 0.1 MPa

Deformation = 3.82 µm

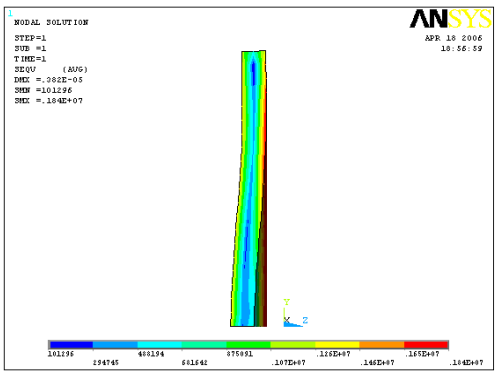

Thermal stress on the cavity wall

Max = 1.84 MPa; Min = 0.1 MPa

Deformation = 3.82 µm

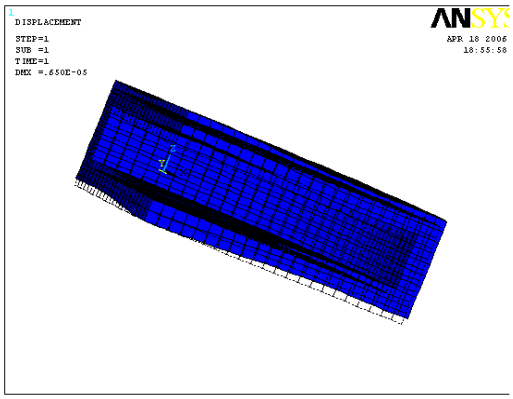

Deformation in the cavity walls

Deformation = 6.5 µm

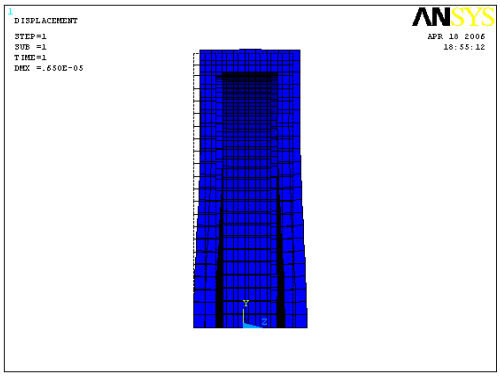

Deformation in the cavity walls

Deformation = 6.5 µm

CHAPTER 8 DISCUSSION & CONCLUSION

This part of the report presents the summary of the work done in dissertation. In this chapter various plots are given to visualize the electromagnetic fields produced by the coil and cavity.

8.1 Coil

The graphs show the magnetic flux density along the central axis of the coil for 2-dimension & 3-dimension simulations are shown below.

Figure 8-1 Plot of flux density along the central axis of the coil

For 42 GHz CW 200 KW gyrotron super conducting coil

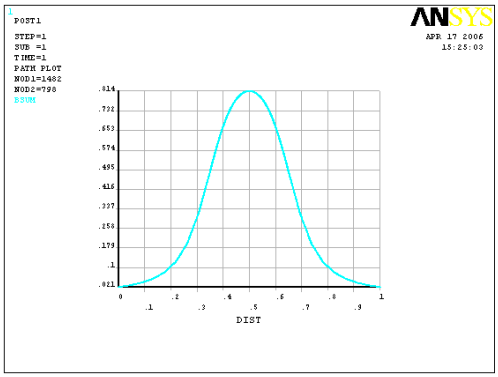

Flux density along the center line of the coil for 2-dimension simulation

Max = 0.814 T

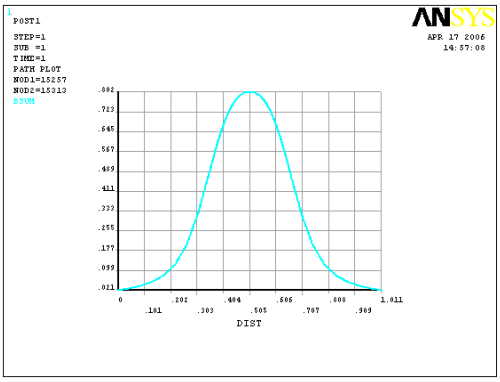

Flux density along the center line of the coil for 3-dimension simulation

Max = 0.802 T

The above graphs indicate that the maximum flux density at the center of the coil is nearer to the design value. The results of the 2-dimensional analysis are more accurate than the 3-dimension. The error in 2D & 3D are 0.2 % & 1.4 % respectively.

Figure 8-2 Plot of flux density along the central axis of the coil

For 110 GHz CW 1 MW gyrotron super conducting coil

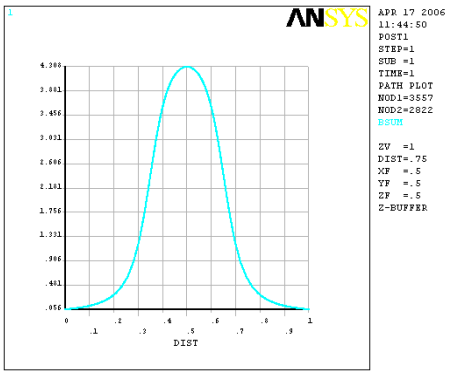

Flux density along the center line of the coil for 2-dimension simulation

Max = 4.308 T

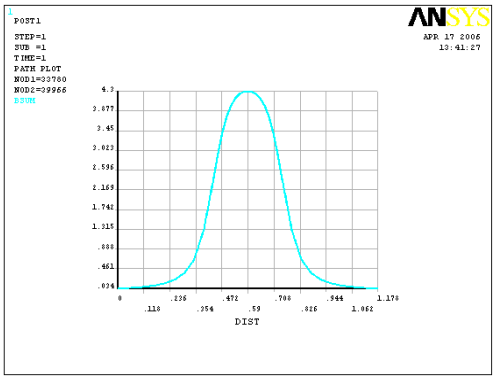

Flux density along the center line of the coil for 3-dimension simulation

Max = 4.3 T

The above graphs indicate that the maximum flux density at the center of the coil is nearer to the design value. The results of the 2-dimensional analysis are more accurate than the 3-dimension. The error in 2D & 3D are 0.1 % & 0.1 % respectively.

8.2 Cavity

The high frequency modal analysis, thermal analysis and structural analysis of CW 200 KW 42 GHz, CW 1 MW 110 GHz and 500 MHz pillbox cavity is done as described in the analysis methodology given in previous chapters. The problems associated in doing the coupled field analysis of cavity in ANSYS software are; the electric & magnetic field results of the high frequency modal analysis are normalized with respect to maximum value. Due to this reason we cannot directly transfer the surface power losses of cavity as heat flux directly to the thermal model to do the thermal analysis. To accomplish this task a macro has been developed. The macro has been tested on a pillbox cavity. The macro, which was written in the APDL code, is presented in the appendix.

The electric and magnetic field patterns of all the cavities are according to the expected modes of operation. The error in the resonant frequency and quality factor in all the cavities are approximately 0.01 % & 0.2 %.

The change in temperature is less than 300^0K for all the cavities, which is below the limit.

The structural analysis is performed on the 500 MHz pillbox cavity. In this case the change in the temperature is 1.346^0 K and the peak effective thermal stress is 1.84 N/mm^2 (MPa), far below copper's yielding stress 55 MPa. These results of the pillbox cavity are in accordance with the reference paper [3].

8.3 Conclusion

A coupled-field analysis process has been established for the cavity design and calculation. The computing is thus simplified and efficiency improved. A test with the pillbox cavity reveals that the computing results would approach theoretical predictions with fine mesh. This process is currently being applied to a cavity in design. It is expected that a good cooling channel layout can thus be obtained.

It has been observed that the calculated resonant frequency approaches to the theoretical value with an error less than 0.01% even at a coarse mesh. But the calculated quality factor can have an error less than 0.1% only at fine mesh. Because Q is related to the stored energy and surface power loss, it means a fine mesh model is necessary when the surface power loss is concerned.

Use of symmetry is one of the easiest ways to reduce a model's size, run time, and memory needs. The effect of symmetry on accuracy was examined for the pillbox model. With a small section of 11.25^0, there is 1% decrease in accuracy.

The electromagnetic results are fairly insensitive to mesh size. Surface heat flux is highly dependent on the mesh density at the vacuum boundary. For this reason, it is advantageous to create a fine mesh in critical areas on the surfaces, while retaining a larger mesh in the body in order to reduce run time and memory usage. This can be achieved by dividing the volume into sub-volumes depending on the local mesh size requirement.

CHAPTER 9 FUTURE SCOPE

The dissertation work is carried out for the static electromagnetic analysis of the super conducting coils and high frequency modal analysis, thermal analysis of the cavities, which are the subsystems of the Gyrotron. This work can be further extended to do thermal, structural and CFD analysis with the help of above results. The thermal loads will cause deformation on structure. Due to this deformation the dimensions get altered which cause a change in operating frequency. Again we have to perform the high frequency modal analysis on the deformed structure to find out whether there is change in operating mode or not. If there is a change then we have to modify the model according to the deformed results.

REFERENCES

1. C. J. Edgcombe, Ed., *Gyrotron Oscillators—Their Principles and Practice*. London, U.K.: Taylor & Francis, 1993.
2. C.S.Lee, S.W.Lee, and S.L.Chuang, "*Plot of modal field distribution in rectangular and circular wave guides*," IEEE trans., microwave theory tech., vol. MTT-33, pp.271-274, 1985.
3. M.C.Lin, Ch.Wang, L.H.Chang, G.H.Luo, and P.J.Chou, "*A coupled-field analysis on RF cavity*," presented at proceedings of the particle accelerator conference, Chicago, 2001.
4. M.Esposito and B.Spataro, "*Use of ANSYS for electromagnetic analysis of RF cavities*," SPARC-RF-05/001, 14th November 2005.
5. M. V. Kartikeyan, E. Borie, B. Piosczyk, and M. Thumm, "*A 42 GHz 200 kW second harmonic gyrotron*," presented at the 27th Int. Infrared and Millimeter Waves Conf., San Diego, CA, Sept. 22–26, 2002.
6. M. V. Kartikeyan *et al.*, "*Conceptual design of a 42 GHz, 200 kW gyrotron operating in the TE mode*," Int. J. Electron., vol. 87, pp. 709–723, 2000.
7. M. V. Kartikeyan, E. Borie, O.Drumm, S.Illy, B. Piosczyk, and M. Thumm, "*Design of a 42 GHz 200 kW Gyrotron operating at second harmonic* ," IEEE Trans., Microwave Theory Tec., Vol.52.No.2 pp 686-692, 2004.
8. M.V.Kartikeyan, "*Preliminary design of a 110 GHz, 1 MW, CW gyrotron*," private communication, 2006.
9. N.Hartman, R.A.Rimmer, "*Electromagnetic, thermal, and structural analysis of RF cavities using ANSYS*," Lawrence berkley national laboratory, Berkley, CA, 2001.
10. Peter A. Rizzi *, Microwave Engineering-Passive circuits*. New jersey , U.S.A, Prentice-Hall, 1999.
11. www.ansys.com

APPENDIX A NOTATIONS, QUANTITIES AND UNITS

Symbol	Quantity	SI Unit	Abbreviation
A	Magnetic vector potential	Weber/meter	Wb/m
B	Magnetic flux density	tesla or weber/meter^2	T or W/m^2
E	Electric field intensity	volt/meter	V/m
D	Electric flux density	coulomb/meter^2	C/m^2
F	Force	Newton	N
H	Magnetic flux intensity	ampere/meter	A/m
J	Current density	ampere/meter^2	A/m^2
L	Inductance	Henry	H
M	Magnetization vector	ampere/meter	A/m
R	Resistance	Ohm	Ω
t	Time	Second	s
V	Electric potential	Volt	V
ε, ε_0	Permittivity	farad/meter	F/m
ε_r	Relative permittivity	(dimensionless)	
μ, μ_0	Permeability	henry/meter	H/m
μ_r	Relative permeability	(dimensionless)	
σ	Conductivity	siemens/meter	S/m
ϕ	Magnetic flux	Weber	Wb

Relative permittivity ε_r of some common materials

$\varepsilon = \varepsilon_r \varepsilon_0$ and $\varepsilon_0 = 8.854 \times 10^{-12}$ F/m

Material	**Relative permittivity, ε_r**	**Material**	**Relative permittivity, ε_r**
Vacuum	1	Dry soil	2.5-3.5
Air (at sea level)	1.0006	Plexi glass	3.4
Stryofoam	1.03	Glass	4.5-10
Teflon	2.1	Quartz	3.8-5
Petroleum oil	2.1	Bakelite	5
Wood (dry)	1.5-4	Porcelain	5.7
Paraffin	2.2	Formica	6
Polyethylene	2.25	Mica	5.4-6
Polystyrene	2.6	Ammonia	22
Paper	2-4	Seawater	72-80
Rubber	2.2-4.1	Distilled water	81
These are low-frequency values at room temperature (20^0 C)			
Note : For most metals, $\varepsilon_r \approx 1$			

Relative conductivity σ of some common materials

Material	**Conductivity,** σ (S/m)	**Material**	**Conductivity,** σ (S/m)
Conductors		***Semiconductor***	
Silver	6.2×10^7	Pure germanium	2.2
Copper	5.8×10^7	Pure silicon	4.4×10^{-4}
Gold	4.1×10^7	***Insulators***	
Aluminum	3.5×10^7	Wet soil	10^{-2}
Tungsten	1.8×10^7	Fresh water	10^{-3}
Zinc	1.7×10^7	Distilled water	10^{-4}
Brass	1.5×10^7	Dry soil	10^{-4}
Tin	9×10^6	Glass	10^{-2}
Lead	5×10^6	Hard rubber	10^{-15}
Mercury	10^6	Paraffin	10^{-15}
Carbon	3×10^4	Mica	10^{-15}
Seawater	4	Fused quartz	10^{-17}
Animal body (average)	0.3	Wax	10^{-17}
These are low-frequency values at room temperature (20^0 C)			

Relative permeability μ_r of some common materials

$\mu = \mu_0 \mu_r$ and $\mu_0 = 4\pi$ X 10^{-7} H/m

Material	**Relative permeability**
Diamagnetic	
Bismuth	0.99983
Gold	0.99996
Mercury	0.99997
Silver	0.99998
Copper	0.99999
Water	0.99999
Paramagnetic	
Air	1.000004
Aluminum	1.00002
Tungsten	1.00008
Titanium	1.0002
Platinum	1.003
Ferromagnetic (nonlinear)	
Cobalt	250
Nickel	600
Mild steel	2000
Iron (pure)	4000-5000
Silicon iron	7000
Mumetal	100000
Purified iron	200000

Maxwell's equation:

General set

Point form	Integral form
$\nabla \times H = J_c + \frac{\partial D}{\partial t}$	$\oint H \cdot dl = \int_S \left(J_c + \frac{\partial D}{\partial t} \right) \cdot dS$ (Ampere's law)
$\nabla \times E = -\frac{\partial B}{\partial t}$	$\oint E \cdot dl = \int_S \left(-\frac{\partial B}{\partial t} \right) \cdot dS$ (Faraday's law; S fixed)
$\nabla \bullet D = \rho$	$\oint_S D \cdot dS = \int_v \rho dv$ (Gauss law)
$\nabla \bullet B = 0$	$\oint_S B \cdot dS = 0$ (nonexistence of monopole)

For free space, where there are no charges ($\rho = 0$) and no conduction currents (Jc=0).

Free-space set

Point form	Integral form
$\nabla \times H = \frac{\partial D}{\partial t}$	$\oint H \cdot dl = \int_S \left(\frac{\partial D}{\partial t} \right) \cdot dS$
$\nabla \times E = -\frac{\partial B}{\partial t}$	$\oint E \cdot dl = \int_S \left(-\frac{\partial B}{\partial t} \right) \cdot dS$
$\nabla \bullet D = 0$	$\oint_S D \cdot dS = 0$
$\nabla \bullet B = 0$	$\oint_S B \cdot dS = 0$

APPENDIX D BENCHMARK PROBLEMS SOLVED

Model 1

Harmonic Analysis of Rectangular Waveguide

Problem specification:

A rectangular wave guide is subjected to a TE_{10} mode loading at one port while the other port is matched. Determine the S-Parameters, power and field solution.

Modeling data:

Dimensions:

Width 'a' = 0.03 m

Height 'b' = 0.01 m

Length 'c' = 0.048 m

Theoretical calculations:

Cutoff frequency

$$f_c = \frac{1}{2\sqrt{\mu\varepsilon}}\sqrt{\left(\frac{m^2}{a^2}+\frac{n^2}{b^2}\right)}$$

$$\lambda_c = \frac{2}{\sqrt{\left(\frac{m^2}{a^2}+\frac{n^2}{b^2}\right)}}$$

Here the dominating mode is TE_{10}, i.e. m = 1, n = 0

$$\lambda_{c_{10}} = \frac{2}{\sqrt{\left(\frac{1}{a^2}+0\right)}} = 0.06m$$

Characteristic impedance:

$$Z_{TE10} = \frac{\eta}{\sqrt{\left(1-\frac{\lambda^2}{\lambda_c^2}\right)}} = \frac{377}{\sqrt{\left(1-\frac{0.0375^2}{0.06^2}\right)}} = 482.946\Omega$$

Scattering parameters:

$$r = \frac{Z - Z_0}{Z + Z_0} = 0.1232\Omega$$

$$S_{11} = S_{22} = r\left(\frac{1 - p^2}{1 - r^2 p^2}\right)$$

$$S_{12} = S_{21} = p\left(\frac{1 - r^2}{1 - r^2 p^2}\right)$$

$p = \exp\left(\frac{-j\omega l}{C_0}\right)$; Where C_0 = Velocity of Light

At port1,	At Port 2,
l = 0 m,	l = 0.048 m,
p = exp(0) = 1	p = exp(-j8.04247)
S_{11} = 0	$S_{21} = 0.991165 \angle -8.83357^0$
S_{12} = 1	S_{22} = 0

ANSYS approach:

In ANSYS, problem is solved with the help of high frequency analysis, in which the excitation is applied with a port load at one end of cable (port 1). The other end of the cable is terminated as matched impedance (port 2). The model is meshed with Hexa sweep mesh.

Inputs:

Properties	**Rectangular waveguide**
Element type	HF 120
Order	Second order element
Permeability	1
Permittivity	1

Load data:

Voltage = 1.0 at input port

Frequency = 8 GHz

ANSYS Results:

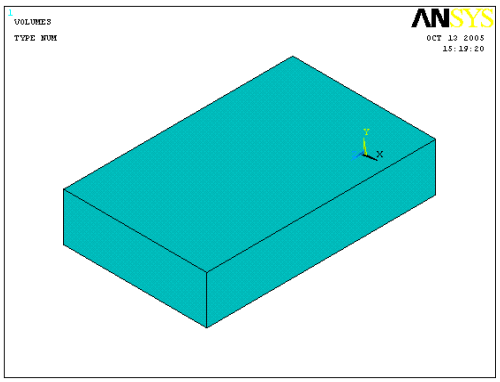

Model of rectangular wave guide

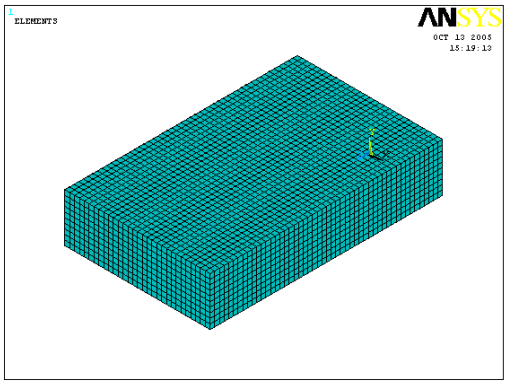

Meshed model

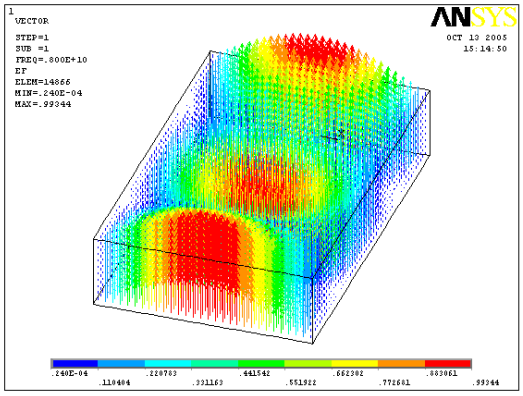

Vector plot of electric field

(Iso. view)

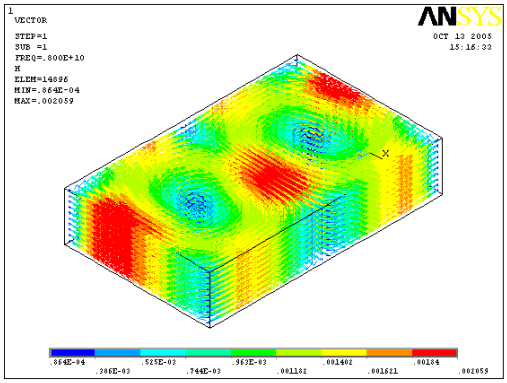

Vector plot of magnetic field

(Iso. view)

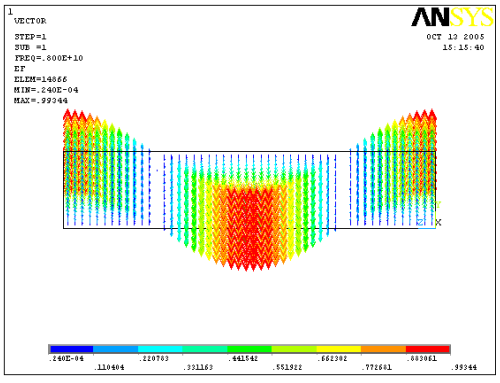

Vector plot of electric field

(Side view)

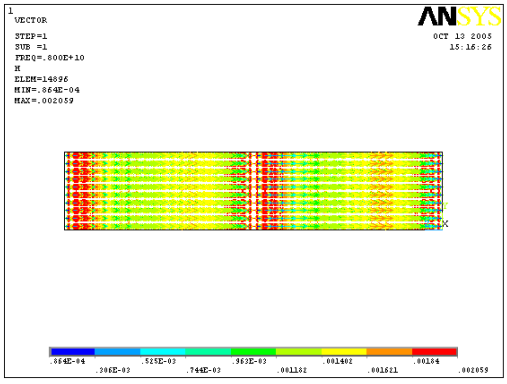

Vector plot of magnetic field

(Side view)

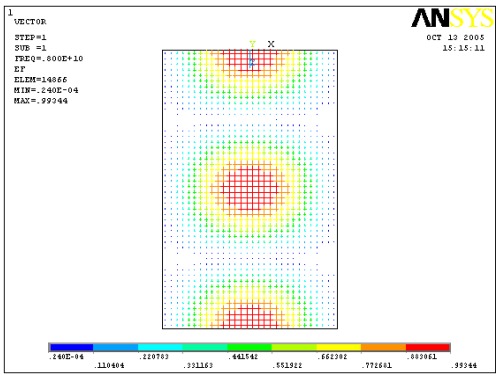

Vector plot of electric field

(Top view)

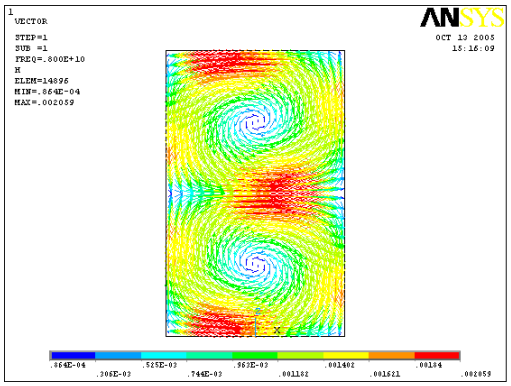

Vector plot of magnetic field

(Top view)

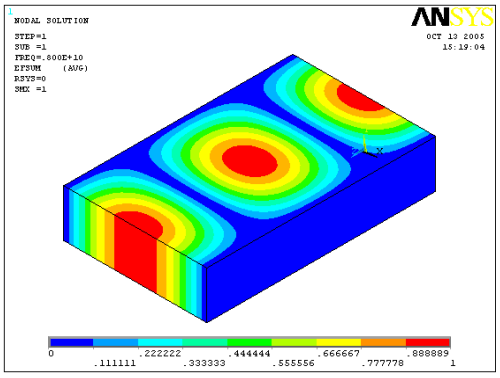

Nodal Solution of electric field

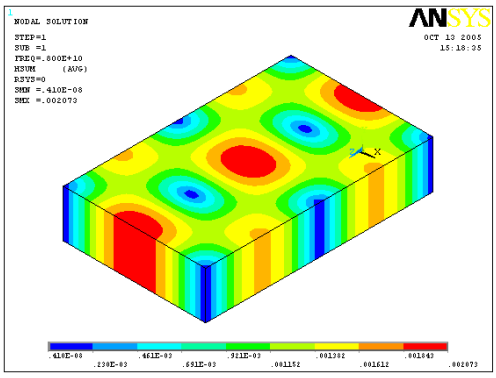

Nodal solution of magnetic field

S-Parameters

Frequency = 8 GHz

Magnitude of S_{11} = 2.456647587E-06

Phase angle of S_{11} = -90.1062953^0

Magnitude of S_{21} = 1.00032332

Phase angle of S_{21} = -0.105582874^0

Model 2

Modal High-Frequency Analysis of Rectangular Cavity

Problem specification:

The problem is to do a modal high-frequency analysis of a rectangular cavity. This analysis calculates the TE_{101} mode eigen frequency in teflon filled cavity with copper walls. It is assumed that the dielectric and surface losses are small and do not affect the eigen frequency solution.

Modeling data:

Dimensions:

Width 'b' = 0.04 m

Height 'a' = 0.03 m

Length 'c' = 1.00 m

Theoretical calculations:

Here $a < b < c$

i.e. $0.3 < 0.4 < 1$, So the dominant mode is TE_{101}

(In TE_{101} the additional subscript indicates that we have chosen the first zero of sin βz that is n = 1. The higher zero gives higher order modes, that is, modes with higher resonant frequencies.)

Resonant frequency:

$$(f_r)_{011} = \frac{1}{2bc}\sqrt{\frac{b^2 + c^2}{\varepsilon\mu}}$$

$$= 0.4036079 \text{ GHz}$$

ANSYS approach:

In ANSYS, problem is solved with the help of modal high frequency Analysis. The block lanczos eigensolver is selected with the frequency range limited to selecting only mode frequencies between 0.35 GHz - 0.55 GHz. The model is meshed with Hexa sweep mesh.

Inputs:

Properties	**Rectangular waveguide**
Element type	HF 120
Order	Second order element
Permeability	1
Permittivity	2.05

Load data:

Applied boundary: Electric wall & shield

Frequency = 0.35 GHz – 0.55 GHz

ANSYS Results:

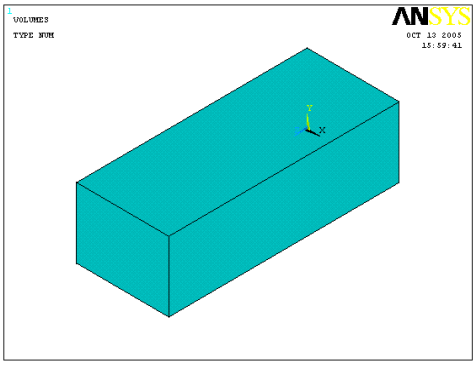

Model of rectangular cavity

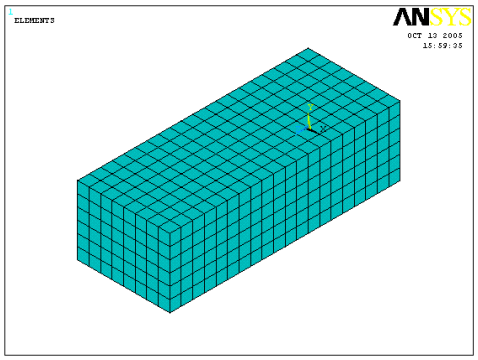

Meshed model

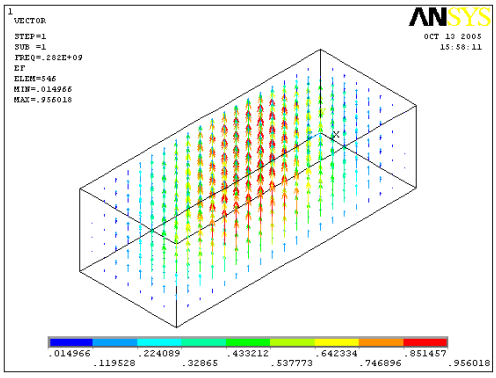

Vector plot of electric field

(*Iso. view*)

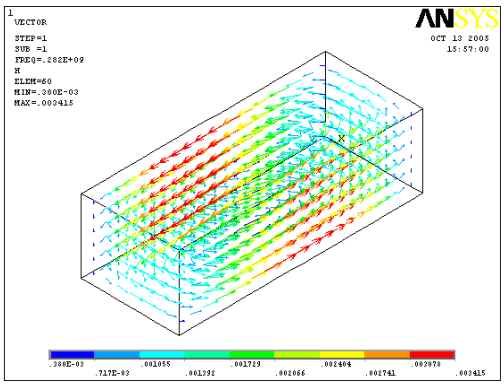

Vector plot of magnetic field

(*Iso. view*)

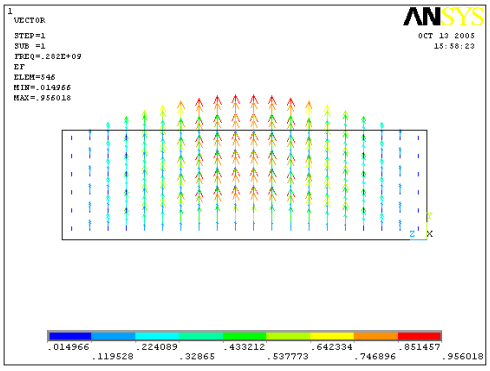

Vector plot of electric field

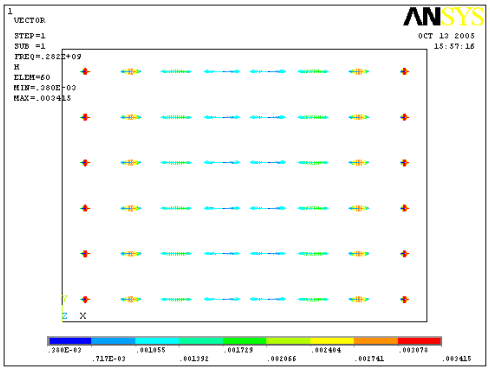

Vector plot of magnetic field

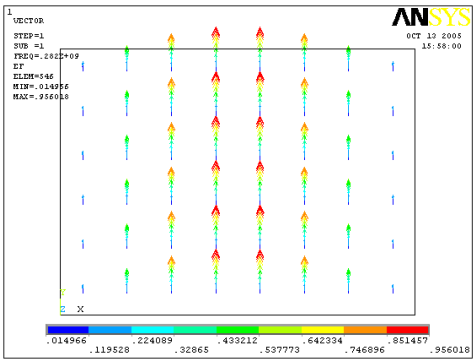

Vector plot of electric field

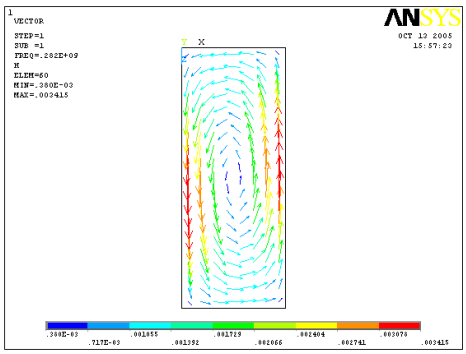

Vector plot of magnetic field

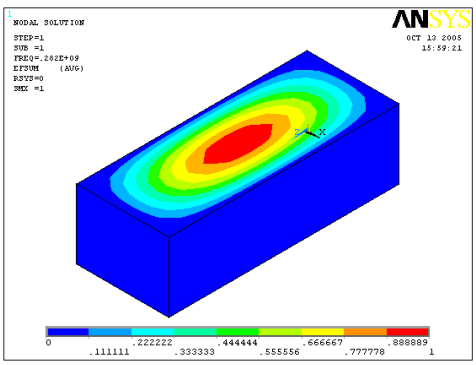

Nodal solution of electric field

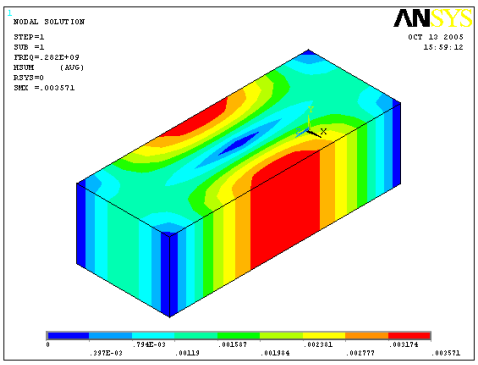

Nodal solution of magnetic field

	Theory	**ANSYS**
Resonant frequency (GHz)	0.40389	0.40392

APPENDIX E MACRO

APDL code:

```
/post1
!file: hex.mac

! select hf120 and surf152 elements
esel,,type,,1
*get,hfmax,elem,,num,max
esel,,type,,2
*get,surfmax,elem,,num,max

! select all nodes attached to surface effect elements
nsel,s,ext
*get,nodemax,node,,num,max

esel,all
nsel,all

! create nodal data array
*dim,nodedata,array,nodemax,20

! initialize column 1 of array to value 2
*do,i,1,nodemax,1
nodedata(i,1)=2
*enddo

! read in elements associated with each node
*do,i,hfmax+1,surfmax,1
*get,n1,elem,i,node,1
*get,n2,elem,i,node,2
*get,n3,elem,i,node,3
*get,n4,elem,i,node,4
```

```
! first node of elem i
location=nodedata(n1,1)
nodedata(n1,location)=i
nodedata(n1,1)=nodedata(n1,1)+1
! second node of elem i
location=nodedata(n2,1)
nodedata(n2,location)=i
nodedata(n2,1)=nodedata(n2,1)+1
! third node of elem i
location=nodedata(n3,1)
nodedata(n3,location)=i
nodedata(n3,1)=nodedata(n3,1)+1
! fouth node of elem i
location=nodedata(n4,1)
nodedata(n4,location)=i
nodedata(n4,1)=nodedata(n4,1)+1
*enddo

! compute sum of H^2*A
h2asum=0

*do,i,1,nodemax,1
 asum=0
 *if,nodedata(i,1),GT,2,then
   *do,j,2,nodedata(i,1)-1,1
    elemnum=nodedata(i,j)
    *get,a,elem,elemnum,area
    asum=asum+a
   *enddo
   aeff=.3333*asum
   *get,hval,node,i,h,sum
   h2asum=h2asum+(hval**2)*aeff
 *endif
*enddo
```

```
! Compute parameters that allow calculation of heat flux
*afun,rad
pi=2*asin(1)
*get,f,active,,set,freq
rad=f*8e-7*pi**2/2*17.24e-9
psum=h2asum*.5*sqrt(rad)
fini

/prep7
! SET POWER dissipated in cavity
c_power=32000

! SET SYMMETRY number
numsymm=4

! Power Scaling Factor
scf=c_power/numsymm/psum

! Prepare to assign heat flux values
! Create array to hold heat flux values at nodes
*dim,heatdata,array,nodemax,1

*do,i,1,nodemax,1
  *if,nodedata(i,1),GT,2,then
    *get,hval,node,i,h,sum
    hflux=scf*.5*sqrt(rad)*hval**2
    heatdata(i)=hflux
  *endif
*enddo

! Assign heat flux values to elements
*do,i,hfmax+1,surfmax,1
*get,n1,elem,i,node,1
*get,n2,elem,i,node,2
```

```
*get,n3,elem,i,node,3
*get,n4,elem,i,node,4

h1=heatdata(n1)
h2=heatdata(n2)
h3=heatdata(n3)
h4=heatdata(n4)

sfe,i,,hflu,,h1,h2,h3,h4
*enddo

!Display heat Fluxes
/sho,,,,8
/psym,cs
/psf,hflu,3
/type,,4
eplot
fini
```